THE ASTROPHYSICAL JOURNAL, 493:730–761, 1998 February 1

CO ($J = 2$–1) LINE OBSERVATIONS OF THE GALACTIC CENTER MOLECULAR CLOUD COMPLEX. II. DYNAMICAL STRUCTURE AND PHYSICAL CONDITIONS

TOMOHARU OKA,[1,2] TETSUO HASEGAWA,[3] MASAHIKO HAYASHI,[4,2]
TOSHIHIRO HANDA,[3] AND SEIICHI SAKAMOTO[5]
Received 1996 October 31; accepted 1997 April 8

ABSTRACT

A large-scale $^{12}C^{16}O$ ($J = 2$–1) survey of the inner few hundred parsecs of the Galaxy has been conducted using the University of Tokyo–Nobeyama Radio Observatory 60 cm survey telescope. We have taken about 700 $^{12}C^{16}O$ ($J = 2$–1) spectra in the region $-2.^\circ5 \leq l \leq 2.^\circ5$ and $|b| \leq 1^\circ$ with $0.^\circ125$ grid spacing, covering the entire region of the huge molecular cloud complex in the Galactic center. We refer to the CO ($J = 1$–0) data taken with the Columbia 1.2 m telescope and calculate the $J = 2$–1 to $J = 1$–0 intensity ratio. Velocity channel maps and longitude-velocity maps of CO ($J = 2$–1) line are presented, with corresponding maps of $J = 2$–1/$J = 1$–0 intensity ratio.

Large-scale CO maps enable us to identify several giant molecular cloud complexes and many characteristic features of molecular gas. We identify 15 molecular cloud complexes larger than $\sim$30 pc in our CO ($J = 2$–1) data. Their virial masses are at least 1 order of magnitude larger than the masses estimated from the CO luminosity. This discrepancy can be removed if we notice that they may not be gravitationally bound but are in pressure equilibrium with the hot gas and/or magnetic field in this region. Using the expressions of virial mass and CO mass for a cloud in the pressure equilibrium case, we get the X-factor for the Galactic center molecular clouds as $X = 0.24 \times 10^{20}$ cm^{-2} (K km s^{-1})$^{-1}$, which is 1 order of magnitude lower than that in the Galactic disk ($X = 3.0 \times 10^{20}$ cm^{-2} [K km s^{-1}]$^{-1}$). We estimate the total molecular mass in the Galactic center as $M(H_2) \cong 2 \times 10^7\ M_\odot$ as a lower limit; the actual total gas mass within the central 400 pc of the Galaxy must be $M(H_2) = (2\text{–}6) \times 10^7\ M_\odot$.

We diagnose the physical conditions of the molecular gas in the Galactic center using the intensity ratio between the $J = 2$–1 and $J = 1$–0 lines. Although the CO $J = 2$–1/$J = 1$–0 line intensity ratio is high ($\sim$0.74) in the midplane, molecular gas at $|b| \geq 0.^\circ25$ exhibits low $J = 2$–1/$J = 1$–0 ratios ($\sim$0.6). The overall $J = 2$–1/$J = 1$–0 luminosity ratio is $R_{(2-1)/(1-0)} = 0.64 \pm 0.01$ if we include all the emission within $|b| \leq 1^\circ$, $-2.^\circ5 \leq l \leq 2.^\circ5$, and $|V_{LSR}| \leq 150$ km s^{-1}. This indicates that low-density gas $\lesssim$50 pc away from the plane dominates the total CO luminosity of the central 400 pc of the Galaxy. The fractional distribution of the molecular gas with $R_{(2-1)/(1-0)}$ for each cloud complex clearly demonstrates the close relationship between the gas with a very high ratio [$R_{(2-1)/(1-0)} \geq 1.0$] and associated UV sources.

Subject headings: Galaxy: center — ISM: clouds — ISM: molecules —radio lines: ISM — surveys

1. INTRODUCTION

Molecular gas is strongly concentrated in the inner few hundred parsecs of the Galaxy (e.g., Bania 1977; Liszt & Burton 1978; Bally et al. 1987, 1988). It seems to form a huge cloud complex with a size of $\Delta l \times \Delta b = 3^\circ \times 1^\circ$, which we call the Galactic center molecular cloud complex. It can be compared with nuclear molecular cloud complexes found near the centers of other galaxies. In the Galactic center molecular cloud complex, gas temperature is known to be relatively high (30–60 K) and roughly uniform over several hundred parsecs (Morris et al. 1983). Emission lines of high-density [$n(H_2) \gtrsim 10^{4-5}$ cm^{-3}] tracer molecules such as CS (Tsuboi et al. 1996), NH_3 (Güsten, Walmsley, & Pauls 1981; Morris et al. 1983), and HCN (Fukui et al. 1977; Jackson et al. 1996) are widely detected over the complex, suggesting that this region contains a large amount of dense molecular gas which leads to active star formation.

Despite the large amount of dense molecular gas, current star formation activity in this complex is known to be not particularly high. For example, a star formation rate (SFR) of 0.3–0.6 $M_\odot$ yr^{-1} (Mezger & Pauls 1979) estimated in the central 100 pc corresponds to a star formation rate per unit gas mass (SFR/M_g), of $\sim 5 \times 10^{-9}$ yr^{-1} if we assume the total gas mass of $M_g = 10^8\ M_\odot$ (Güsten 1989). This is only about 3 times larger than that in the solar neighborhood ($\cong 1.5 \times 10^{-9}$ yr^{-1}) and no more than a half of that in the molecular ring of the Galaxy ($\cong 10^{-8}$ yr^{-1}). On the other hand, X-ray emission from the Galactic center suggests that 1000 supernova explosions have occurred in the last 10^4 yr (Yamauchi et al. 1990), which points out the possibility that the center of the Galaxy has experienced an active star-forming phase in the recent past.

An important issue is the estimate of the total gas mass in the central 500 pc. ^{12}CO observations give very large total molecular mass, $M_g = (1\text{–}3) \times 10^8\ M_\odot$ (Bania 1986; Güsten 1989), if we adopt the standard conversion factor $X \equiv N(H_2)/W_{CO} = 3 \times 10^{20}$ cm^{-2} (K km s^{-1})$^{-1}$ (Young & Scoville 1991). Mapping observations of less opaque ^{13}CO

[1] Cosmic Radiation Laboratory, the Institute of Physical and Chemical Research (RIKEN), 2-1 Hirosawa, Wako, Saitama 351-01, Japan; oka@postman.riken.go.jp.
[2] Department of Astronomy, Faculty of Science, University of Tokyo, 7-1-1 Hongo, Bunkyo-ku, Tokyo 113, Japan.
[3] Institute of Astronomy, Faculty of Science, University of Tokyo, 2-21-1 Osawa, Mitaka, Tokyo 181, Japan.
[4] National Astronomical Observatory, 2-21-1 Osawa, Mitaka, Tokyo 181, Japan.
[5] Nobeyama Radio Observatory, Nobeyama, Minamimaki, Minamisaku, Nagano 384-13, Japan.

(Bally et al. 1988) and H_2CO (Zylka et al. 1992) lines also yields $M_g \sim 10^8\ M_\odot$. However, the lack of excess hard γ-ray emission toward the Galactic center region gives an upper limit to the total gas mass of $5.8 \times 10^7\ M_\odot$ (Blitz et al. 1985). From a careful analysis of far-infrared/submillimeter spectrum of the Galactic center, Cox & Laureijs (1989) derived $M_g(R \leq 750\ \mathrm{pc}) \cong 6 \times 10^7\ M_\odot$. These mass estimates sharply conflict with the results from molecular line observations. We note that the total gas mass estimated from γ-ray and FIR/submillimeter data gives a SFR/M_g value in the Galactic center similar to or larger than that in the molecular ring of the Galaxy ($R = 4$–6 kpc).

Understanding of the physical conditions in the molecular gas and their possible connection with the star formation would be crucial to unveil the star formation history in this region. In order to investigate the present-day status of the molecular gas in the central few hundred parsecs of the Galaxy, we have made a large-scale mapping in the CO ($J = 2$–1) emission using the University of Tokyo–Nobeyama Radio Observatory (NRO) 60 cm Survey telescope. The beam size of the telescope (9′) is close to that of the 1.2 m telescope used in the Columbia CO ($J = 1$–0) Survey at 2.6 mm. The matched beam size is essential for the direct comparison of the intensities. The main purpose of our CO ($J = 2$–1) survey is to reveal a large-scale variation of physical conditions in molecular clouds with the place in the galaxy, especially a difference in physical conditions between molecular gas in the Galactic center region and those in the Galactic disk, in terms of the $J = 2$–$1/J = 1$–0 intensity ratio.

While the CO ($J = 1$–0) line emission traces the distribution of low-density molecular gas [$n(H_2) \gtrsim 3 \times 10^2\ \mathrm{cm}^{-3}$], the CO ($J = 2$–$1$) line emission traces the gas distribution of slightly higher density [$n(H_2) \gtrsim 10^3\ \mathrm{cm}^{-3}$]. These lines do not reflect the gas column density linearly because they are highly saturated ($\tau \gtrsim 10$) toward central regions of molecular clouds. However, these lines sensitively trace less opaque low-density cloud envelopes. Since a major fraction of the mass in a molecular cloud resides in their envelopes, the intensities of these lines provide rough measures of the total molecular mass, with slight difference in their most sensitive density ranges. Assuming that the emitting regions of these two lines are roughly identical, we can diagnose the physical conditions in the cloud envelopes using the $J = 2$–$1/J = 1$–0 intensity ratio.

Oka et al. 1996a (Paper I) has presented preliminary results of our observations along the galactic plane and discussed star formation history in the central few hundred parsecs. This paper presents two-dimensional mapping data of $^{12}CO^{16}O$ ($J = 2$–1) line emission. Based on these data, we discuss the distribution of CO ($J = 2$–1) emission and the $J = 2$–$1/J = 1$–0 intensity ratio, and present identification of molecular cloud complexes larger than 30 pc in the Galactic center in § 3. Then we discuss their dynamical equilibrium state using CO luminosity-virial mass plot. By noticing that the cloud complexes in the Galactic center may be in equilibrium with external pressure, we derive a new estimate from ^{12}CO line for the molecular mass in the Galactic center region, which agrees with the smaller mass estimates based on the γ-ray, far-infrared, and $C^{18}O$ observations. In § 4, we discuss the difference in physical conditions between the molecular gas in the Galactic center and that in the Galactic disk, as well as differences between the individual Galactic center molecular clouds based on the $J = 2$–$1/J = 1$–0 intensity ratio. Throughout this paper we adopt $D = 8.5$ kpc as the distance to the Galactic center.

2. OBSERVATIONS AND DATA ANALYSIS

The CO ($J = 2$–1) mapping observations of the Galactic center region were made during the period from 1992 December to 1993 March (season 1), and from 1995 January to March (season 2) using the Tokyo-NRO 60 cm telescope at Nobeyama Radio Observatory (Hayashi et al. 1990). About 700 spectra of $^{12}C^{16}O$ (hereafter CO) $J = 2$–1 line were obtained in the region $-2\overset{\circ}{.}5 \leq l \leq +2\overset{\circ}{.}5$, $-1^\circ \leq b \leq +1^\circ$, with a spacing of $0\overset{\circ}{.}125$ ($7\overset{\prime}{.}5$). During the observing season 1, we used a cooled Schottky diode mixer as a receiver frontend. The typical system temperature ranged from 1000 to 1500 K (SSB) including the atmospheric loss. During the season 2, we utilized a newly developed SIS receiver. Typical system noise temperature of the SIS receiver was improved to 800–900 K including the atmospheric loss. The HPBW of the telescope is $9' \pm 1'$ at the CO ($J = 2$–1) frequency (230.538001 GHz), which corresponds to 20 pc at the distance of the Galactic center of 8.5 kpc. The telescope with an offset Cassegrain optics has main-beam efficiencies including forward spillover and scattering ($\eta_{\mathrm{MB}}\,\eta_{\mathrm{fss}}$, Kutner & Ulich 1981) as high as $91\% \pm 3\%$ for the Schottky receiver and $83\% \pm 3\%$ for the SIS receiver, respectively. The pointing accuracy of the telescope was checked by tracking bright stars and was good to 1′ (rms) in both azimuth and elevation.

Calibration of antenna temperature was accomplished by chopping between an ambient temperature load and the sky. Reproducibility of intensity was checked by observations of the standard position (l, b) = (0°, 0°), and was found to be good to 7% (1 σ) in season 1, and 9% (1 σ) in season 2. Monitoring the standard calibration source Orion KL over the seasons, we found the intensity of Orion KL was well reproduced to 7% (1 σ) in season 1 and 8% (1 σ) in season 2. These dispersions are quite consistent with those of the standard position in the Galactic center. The intensity scales in the two observing seasons are quite consistent within the measuring accuracy of the beam efficiencies. We also found that the intensity scale show no elevation dependence, even at low elevations (EL = 15°–25°) where we observe the Galactic center.

Spectra were obtained with a 2048 channel acousto-optical spectrometer (AOS) which covers an instantaneous bandwidth of 250 MHz with a spectral resolution of 330 kHz. At 230 GHz, these correspond to 330 km s^{-1} velocity coverage and 0.43 km s^{-1} velocity resolution, respectively. The instantaneous bandwidth was sometimes insufficient to cover the full velocity extent of the CO emission from the Galactic center. For these cases we took spectra covering adjacent velocity ranges with enough overlaps to determine the baseline levels.

All data were obtained by position switching between target positions and reference positions. Reference positions were taken at the Galactic latitude $b = -3°$, where no significant CO ($J = 2$–1) emission was detected, and their longitudes were chosen dynamically so that the reference positions were to be at the same elevations (within $\Delta EL \leq \pm 0\overset{\circ}{.}3$) as the target positions in order to minimize baseline ripples. Integration time was typically 100 s on source for the Schottky receiver and typically 50 s for the SIS receiver. The rms noise of each spectrum was less than 0.2 K on the T_A^* scale. The overall accuracy of the intensity scale is better

than ± 0.3 K (due to baseline uncertainties) or $\pm 8\%$ (due to intensity and efficiency calibration errors). In some positions the velocity extent of the emission is too large to be covered by the limited bandwidth of AOS, and determination of the baseline level is difficult. In such case, the intensity scale of the CO ($J = 2$–1) emission tends to be underestimated by up to ~ 1 K. Some CO ($J = 2$–1) spectra toward the Galactic center taken with the system have been presented in Paper I.

All data in this survey were reduced with STAR reduction package developed by us. After flagging out some bad scans, spectra of each position were averaged. Baselines were subtracted by fitting linear lines, or if necessary, by the lowest degree polynomial that produce straight baseline in the range where emission is known not to be present. The highest degree of polynomial is 6, but this is for only a few exceptional cases. About one-third of the spectra required nonlinear polynomial fits, and most of them have been successfully fitted by second or third polynomial baseline. Channels contaminated by an internal interference of the receiver were touched up with a linear interpolation from outer five chanels in both sides.

To get plausible distribution of the intensity ratio, it was necessary to correct relative pointing error between the $J = 2$–1 and $J = 1$–0 observations. We calculated the first-order moment of integrated intensity (center of intensity) in each line along the Galactic latitude and longitude, then found a systematic displacement along the latitude. The displacements were less than 5′ in latitude and were well fitted with a second-order polynomial of the Galactic longitude within $\pm 1'$ accuracy. No displacement exceeding 1′ in the longitudinal direction was found. We corrected this latitudinal displacement at each longitude using the following transformations:

$$T_{1-0}(l, b) = \sum_{(i,j)} T_{1-0}(l_i, b_j) \exp\{-[(l-l_i)^2 + (b-b_j)^2]/\sigma^2\} \left(\sum_{(i,j)} \exp\{-[(l-l_i)^2 + (b-b_j)^2]/\sigma^2\}\right)^{-1},$$

$$T_{2-1}(l, b) = \sum_{(i,j)} T_{2-1}(l_i, b_j) \times \exp\{-[(l-l_i)^2 + (b-b_j-\Delta b)^2]/\sigma^2\} \left(\sum_{(i,j)} \exp\{-[(l-l_i)^2 + (b-b_j-\Delta b)^2]/\sigma^2\}\right)^{-1}, \quad (1)$$

where σ is a smoothing radius, which was set to 9′. We employed the regressed expression to the second-order polynomial of l for the latitudinal displacement $\Delta b(l)$. The final resolutions of the transformed maps are 12.′6 (9′ beam + 9′ Gaussian smoothing).

3. RESULTS

3.1. *The Data*

The full results of the CO ($J = 2$–1) survey are presented in Figures 1 and 2 as sets of l-b and l-V maps with the corresponding maps of the $J = 2$–1 to $J = 1$–0 line intensity ratio $R_{(2-1)/(1-0)} \equiv I_{\mathrm{CO}(2-1)}/I_{\mathrm{CO}(1-0)}$. The line intensity maps are in units of main-beam temperature T_{MB} ($\equiv T_{\mathrm{A}}^*/[\eta_{c,\mathrm{MB}}\eta_{\mathrm{fss}}]$).

Figure 1 presents a full set of velocity channel maps for the CO ($J = 2$–1) line emissivity in the Galactic center and the corresponding maps of $R_{(2-1)/(1-0)}$, the maps covering the velocity range $V_{\mathrm{LSR}} = -150$ km s^{-1} and ending at $+150$ km s^{-1}. CO ($J = 2$–1) line emissivity maps show the spatial distribution of the line intensity integrated over successive 10 km s^{-1} wide velocity range. The intensity ratio is calculated in the region where the CO ($J = 1$–0) line integrated intensity exceeds 20 km s^{-1}.

Figure 2 presents a full set of longitude-velocity diagrams (l-V) diagrams for the CO ($J = 2$–1) line emission and those of $R_{(2-1)/(1-0)}$ for each of the galactic latitudes observed in our survey. The maps cover the longitude range $l = -2.^\circ5$ to $+2.^\circ5$, and the velocity range $V_{\mathrm{LSR}} = -150$ km s^{-1} to $+150$ km s^{-1}. The resolutions in these l-V maps are $\Delta l \times \Delta V = 12.'6 \times 5$ km s^{-1}. The intensity ratio is calculated in the region where the CO ($J = 1$–0) line temperature exceeds 2 K after binning to a velocity resolution of $\Delta V = 5$ km s^{-1}.

3.2. *Overview of the Results*

Emission from the Galactic center molecular cloud complex dominates the maps. The foreground arms appear in the l-V maps as narrow absorption features at $V_{\mathrm{LSR}} \cong 0$, -30, -50 km s^{-1} against the strong emission from the Galactic center, or weak emission features in the larger absolute latitudes. These foreground features can easily be distinguished from the Galactic center molecular clouds by their narrow velocity widths ($\Delta V \leq 5$ km s^{-1}) and by their longitudinal continuity as well as their high latitudinal scale heights. We focus in this paper on the strong emission from the molecular clouds in the Galactic center.

The longitudinal and latitudinal distributions of CO ($J = 2$–1) line emission and $R_{(2-1)/(1-0)}$ are discussed in §§ 4.1 and 4.2. Although most of the Galactic center molecular clouds appear within the permitted velocity range for the galactic rotation ($l > 0^\circ$, $V_{\mathrm{LSR}} > 0$ km s^{-1} and $l < 0^\circ$, $V_{\mathrm{LSR}} < 0$ km s^{-1}), large amounts of molecular gas appear at the forbidden velocities ($l > 0^\circ$, $V_{\mathrm{LSR}} < 0$ km s^{-1} and $l < 0^\circ$, $V_{\mathrm{LSR}} > 0$ km s^{-1}). Some of these forbidden velocity clouds will be identified as parts of the feature known as "expanding molecular ring" (EMR; Kaifu, Kato, & Iguchi 1972; Scoville 1972).

3.3. *Galactic Center Molecular Clouds*

The Galactic center molecular cloud complex consists of a number of giant molecular clouds with scales ranging from 20 to 50 pc[6]. We made a catalog of these molecular clouds in the Galactic center region identified with our 9′ resolution (Table 1). We tabulated their peak positions, extents (FWHM), peak main-beam temperatures, and other cloud parameters.

Each molecular cloud in Table 1 contains a single peak exceeding 2 K in main-beam temperature at our 9′ resolution. We defined their widths (Δl, Δb, and ΔV) as full widths at half-maximum (FWHM) of the main-beam temperature. Integrated intensities tabulated in Table 1 are calculated by integrating the data which is brighter than the half of the peak value within the full extents ($\Delta l \times \Delta b \times \Delta V$) of each cloud. The sum of the CO luminosities picked up as these clouds ($L_{\mathrm{CO,cloud}} \cong 9 \times 10^6$ K km s^{-1} pc^2) amounts only $\sim 20\%$ of the total CO luminosity from this region

[6] In this paper we call them clouds, although it is possible that they are actually complexes of clouds.

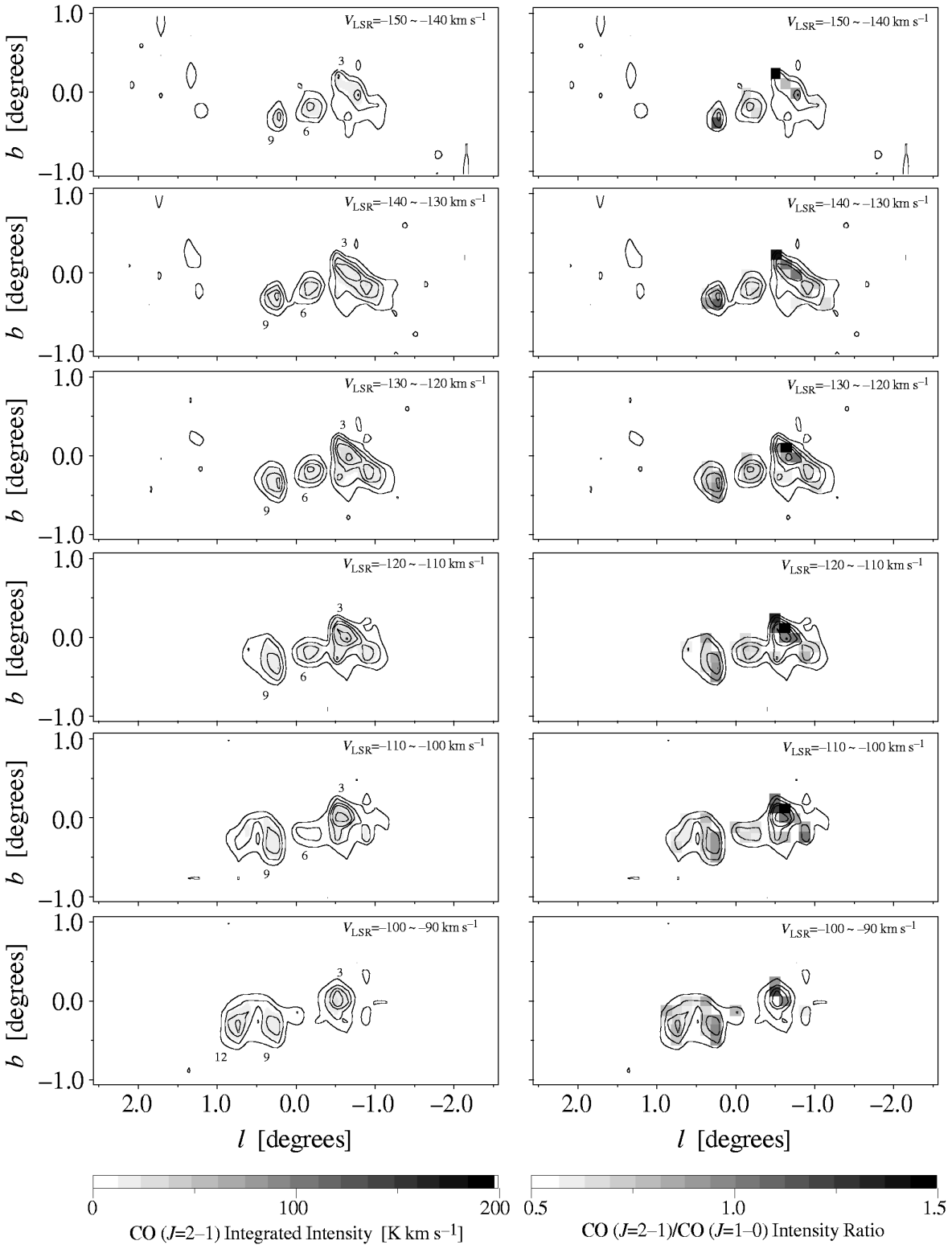

FIG. 1.—Velocity channel maps of CO (J = 2–1) line emissivity with the corresponding maps of the J = 2–1/J = 1–0 intensity ratio. Each map covers a velocity interval of 10 km s^{-1}, starting with V_{LSR} = −150 km s^{-1} and ending at +150 km s^{-1}. Contour levels for the J = 2–1 line emissivity are set at arbitrary intervals, 5, 10, 15, 20, 30, 40, 60, 80, 100, 120, 140, 160, 180, and 200 K km s^{-1}.

($L_{CO,tot} \cong 5 \times 10^7$ K km s^{-1} pc^2). This means that these clouds do not represent the overall characteristics of the molecular gas in the Galactic center. The intensity ratios of the identified clouds tend to be higher than that of intercloud-complex gas, which dominates the total CO luminosity.

When peaks of the CO emission are well separated in the $l \times b \times V$ space, cloud identification as well as the measure-

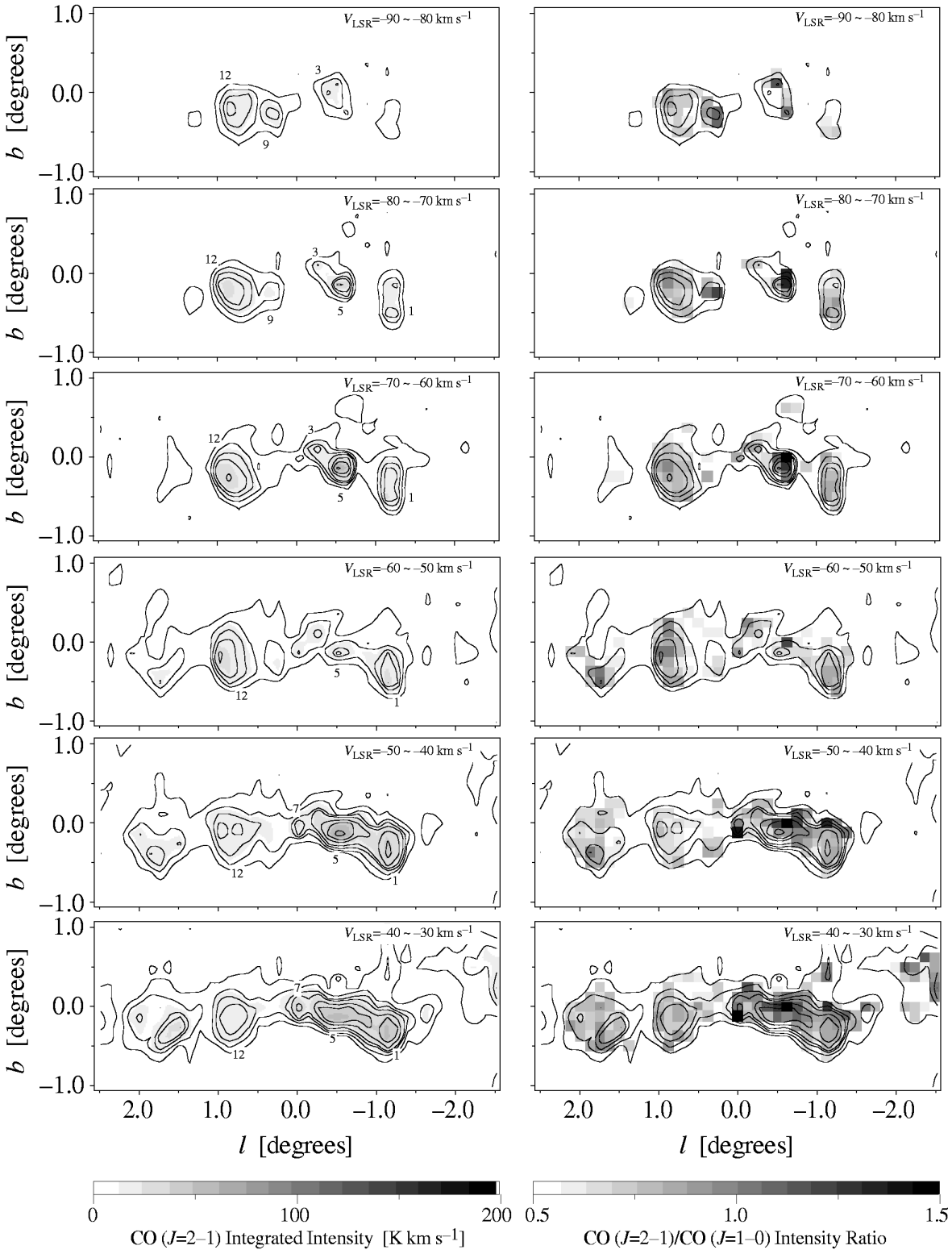

FIG. 1—*Continued*

ment of the sizes and line widths of the clouds is straightforward. As the cloud-to-cloud separation decreases, however, blending of cloud emission becomes a potential problem. In an extreme case, two unrelated clouds seen along a line of sight could have radial velocities close to each other by chance (e.g., one in the near side and the other in the far side), and this blend of clouds may be identified as one big cloud. For the present case, the identified clouds occupy $\Delta l \times \Delta b \times \Delta V$ volume of 90 (deg^2 km s^{-1}), which is ~25% of that of the densest region in the Galactic center molecular cloud complex (3° × 0°.6 × 200 km s^{-1}), and hence the probability of the cloud overlap within the half-intensity

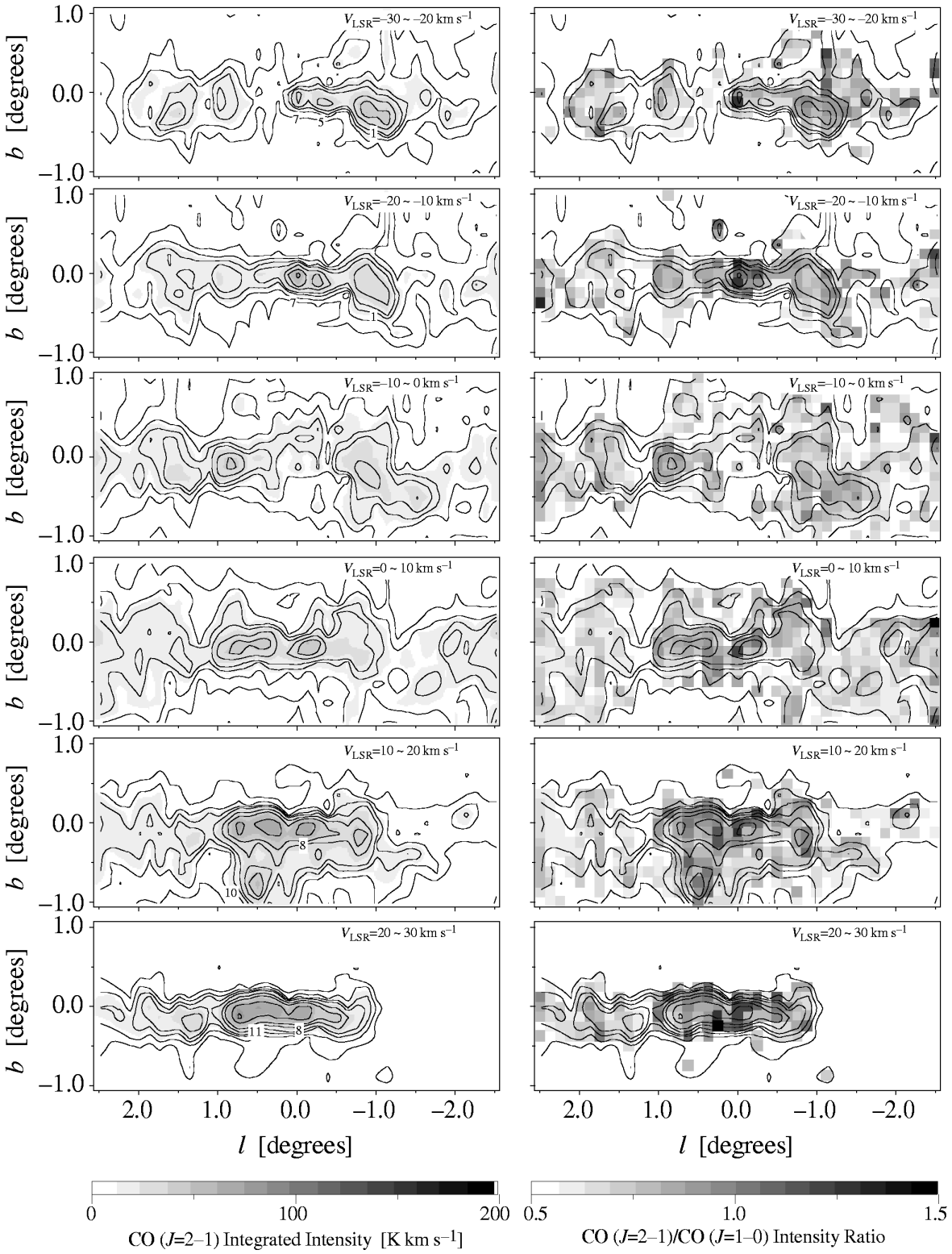

FIG. 1—*Continued*

point is fairly low (~6%). The tenuous CO emission fills the space between the clouds with low brightness. The identified clouds are distinctly brighter, and many of them exhibit higher $R_{(2-1)/(1-0)}$ as we will see later. We believe that most of them are real clouds or cloud complexes (i.e., well-defined regions of higher gas density), although they may not be gravitationally bound (see § 5).

Virial masses in Table 1 are calculated from the tabulated quantities using the following standard formula (Solomon et al. 1987).

$$M_{VT} = 3 f_p \frac{S\sigma_V^2}{G}, \quad (2)$$

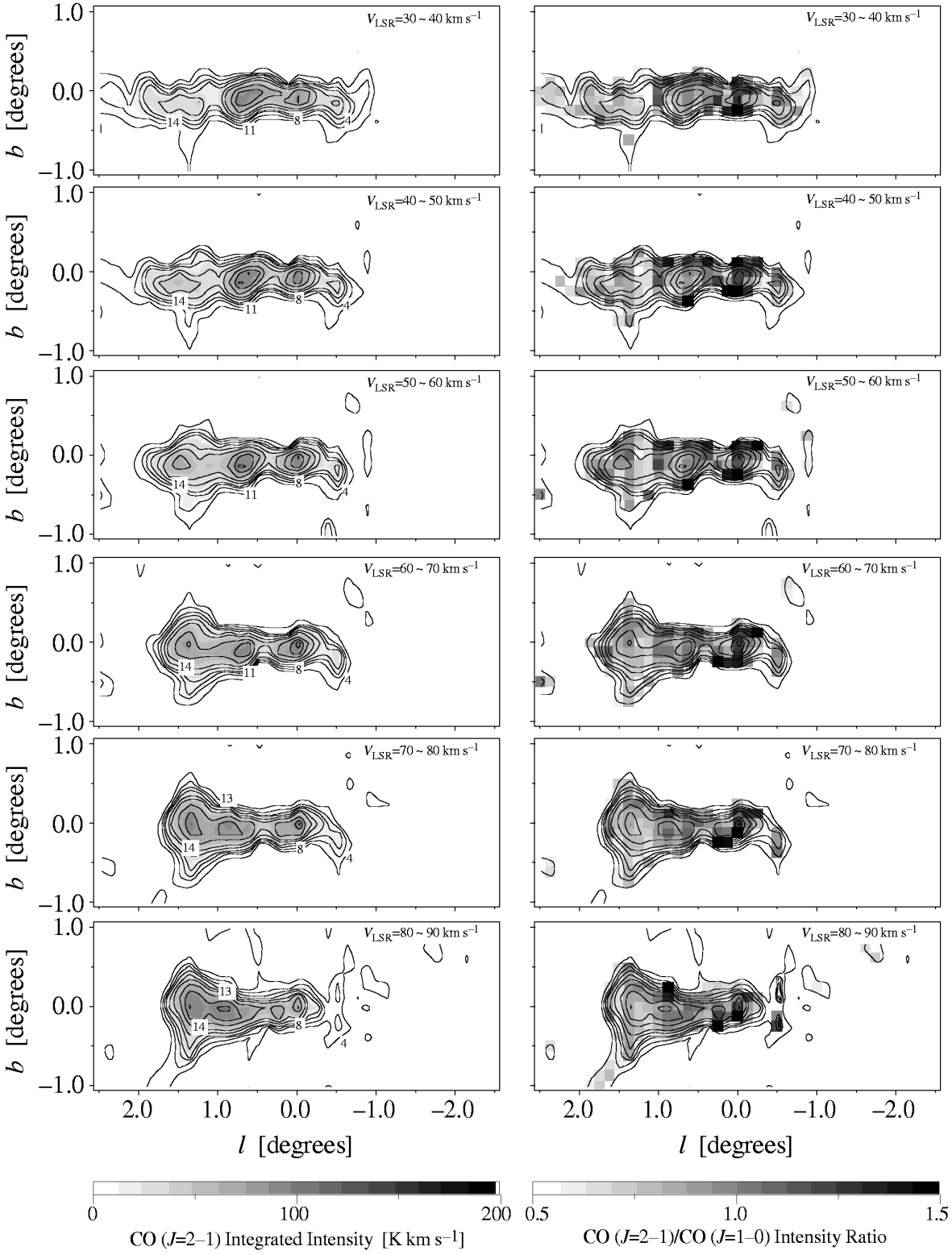

FIG. 1—*Continued*

where S is the size parameter defined as $S = D \tan (\sigma_l \sigma_b)^{1/2}$, D (= 8.5 kpc) is the distance to the Galactic center, and f_p is a projection factor. We take $f_p = 2.9$ that corresponds to the case of $a = 1.0$, where a is the exponent of the density profile, $\rho(r) \propto r^{-a}$. We converted the FWHMs of main-beam temperature to equivalent sizes and velocity dispersions (σ_l, σ_b, and σ_v) by multiplying 0.42 [$= 1/2(2 \ln 2)^{1/2}$]. We will see in § 5.1 that the choices of cloud definition lead no essential difference in the statistical characteristics of molecular clouds. CO masses in the table are calculated from the CO luminosities using the standard conversion factor $X \equiv N(H_2)/I_{CO} = 3.0 \times 10^{20}$(cm^{-2} [K km s^{-1}]$^{-1}$) (Young & Scoville 1991). Short descriptions of the individual clouds follows.

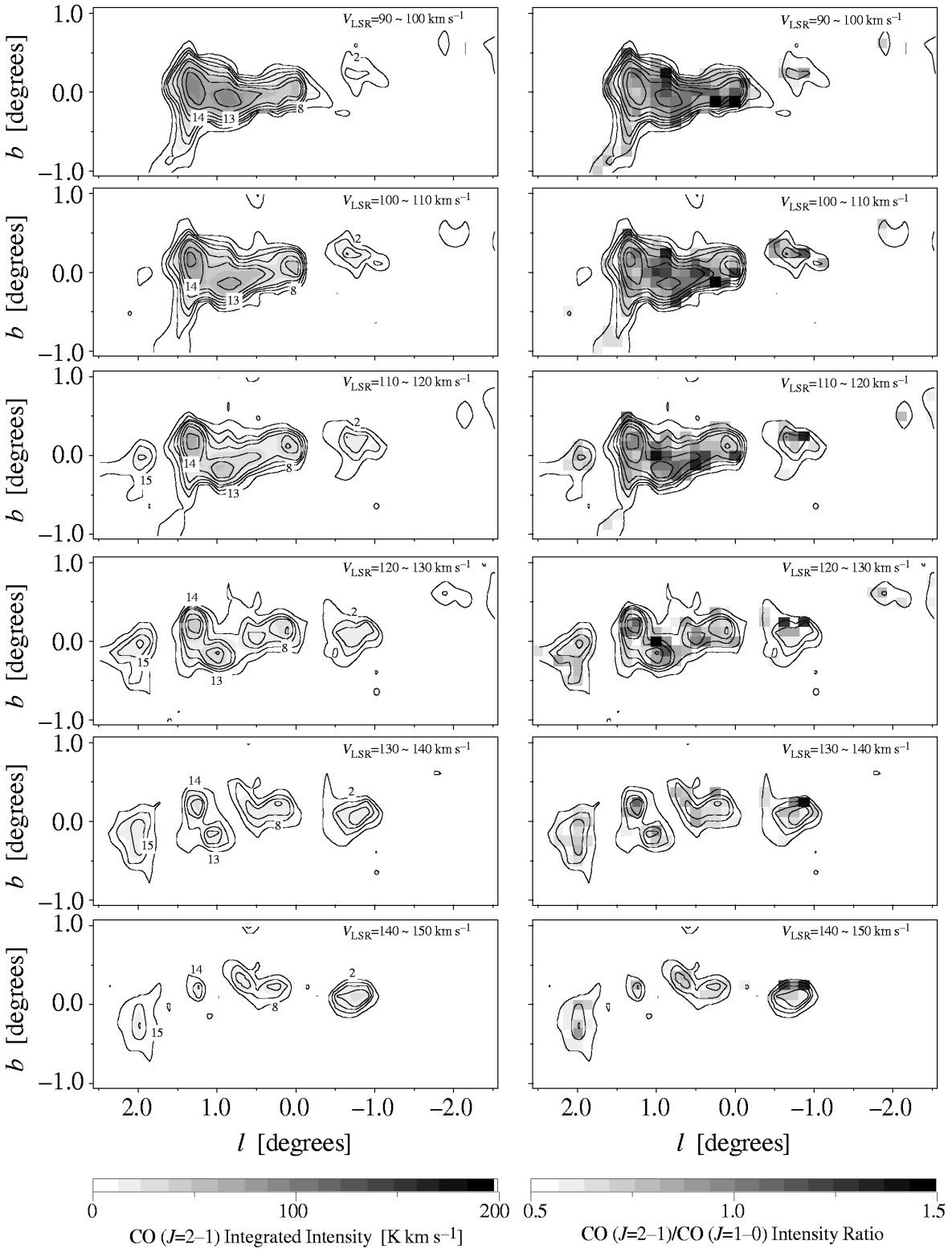

FIG. 1—*Continued*

Cloud 1 [*CO 358.9−0.4(−30)*].—This cloud appears at $(l, b, V_{LSR}) \cong (-1.^{\circ}125, -0.^{\circ}375, -30$ km s$^{-1})$. The intensity ratio is $R_{(2-1)/(1-0)} = 0.7$–0.9 over the cloud, and the mean ratio is $R_{(2-1)/(1-0)} = 0.85$.

Cloud 2 [*CO 359.2+0.1(+150)*].—This cloud is best seen in our data in the *l-V* plane at $b = 0.^{\circ}125$, as an isolated feature at $(l, b, V_{LSR}) = (-0.^{\circ}75, 0.^{\circ}125, 130$ km s$^{-1})$. It is one of the clouds which compose the EMR. The mean intensity ratio is $R_{(2-1)/(1-0)} = 0.71$. We suspect that the very high ratio at $b = 0.^{\circ}25$ might be an artifact of residual relative pointing error.

Cloud 3 [*CO 359.4+0.0(−120)*]. This cloud is associated with a radio source Sgr C, an H II region with two velocity components at $V_{LSR} = -59$ km s^{-1} and -120 km s^{-1}

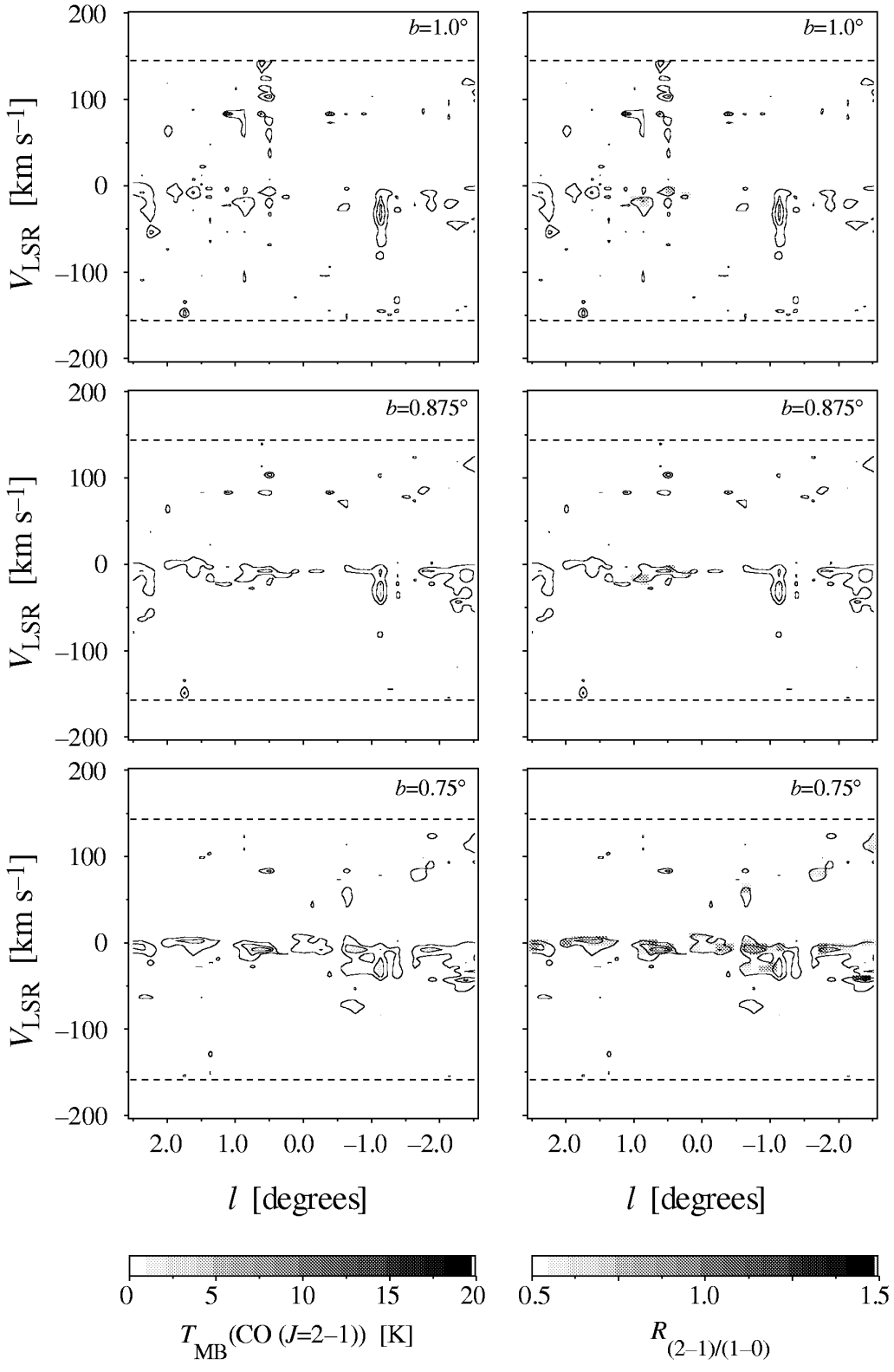

FIG. 2.—Longitude-velocity diagrams (l-V diagrams) of CO ($J = 2$–1) line main-beam temperature with the corresponding maps of the $J = 2$–1/$J = 1$–0 intensity ratio, each covering the range $V_{LSR} = -150$ km s^{-1} to $+150$ km s^{-1} and $l = -2.^{\circ}5$ to $+2.^{\circ}5$. Contours for the $J = 2$–1 line temperatures are drawn at 0.5, 1, 1.5, 2, 3, 4, 6, 8, 10, 12, 14, 16, 18, and 20 K.

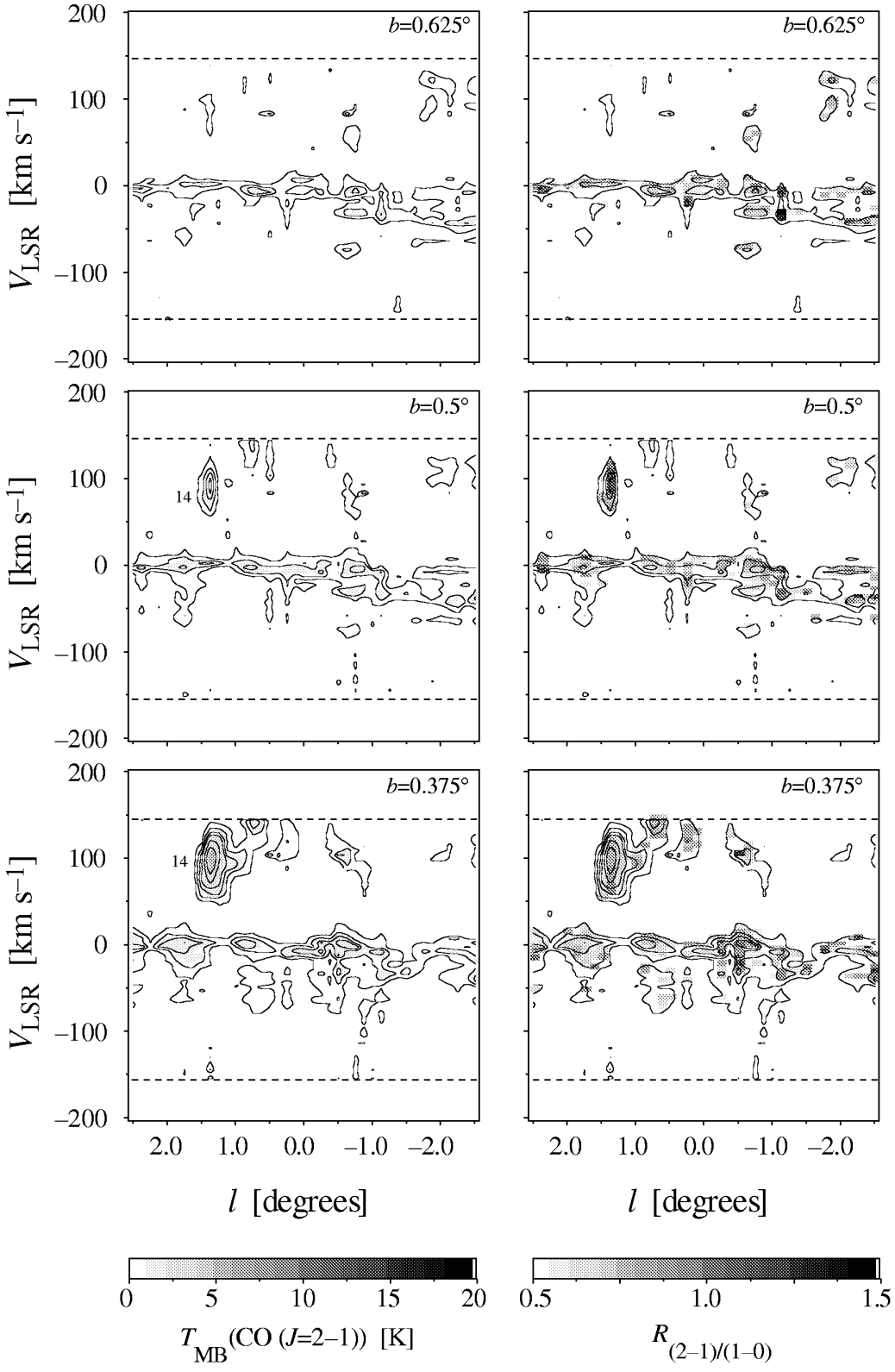

FIG. 2—*Continued*

(Pauls & Mezger 1975). It appears as a well-isolated feature in the *l-V* diagram at $b = 0°$ centering at (l, b, V_{LSR}) = ($-0°.625$, $0°.0$, -120 km s^{-1}). The intensity ratio is $R_{(2-1)/(1-0)} = 0.6$–0.8 near the cloud center. Very high ratios at $b = 0°.25$ might be artificial. The mean intensity ratio is $R_{(2-1)/(1-0)} = 0.84$.

Cloud 4 [*CO 359.5−0.3(+30)*].—This cloud appears at (l, b, V_{LSR}) $\cong$ ($-0°.5$, $-0°.25$, 30 km s^{-1}) with a wing-

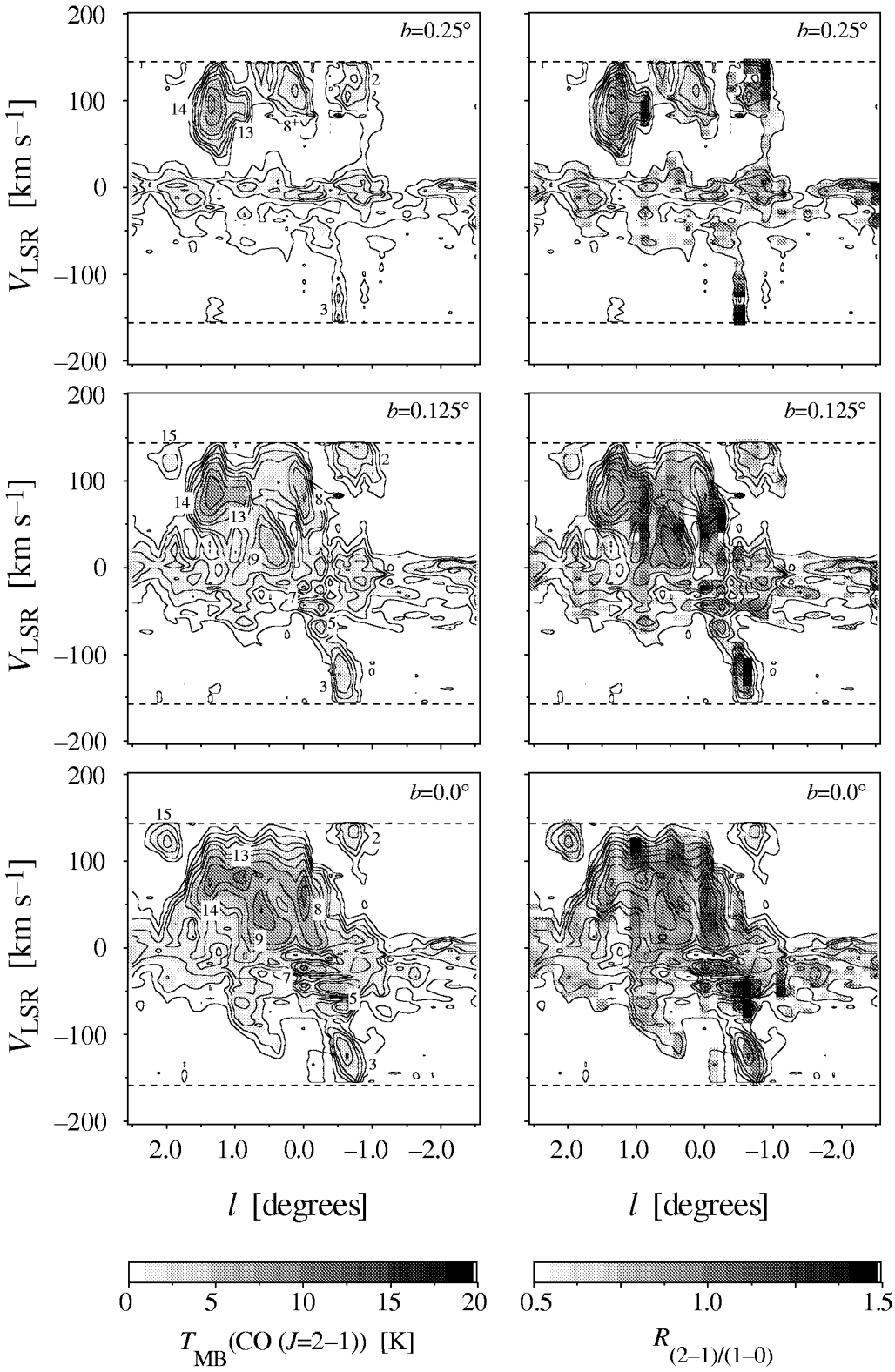

FIG. 2—*Continued*

shaped appearance in the *l*-*V* plane. It is associated with some spurlike features out of the plane at (l, b, V_{LSR}). The mean intensity ratio is $R_{(2-1)/(1-0)} = 0.81$.

Cloud 5 [*CO 359.5+0.0*(−35, −65)].—This cloud is divided into two velocity components by the absorption feature at $V_{LSR} \cong -50$ km s^{-1} (3 kpc arm). The intensity ratio seems to be high ($R_{(2-1)/(1-0)} \geq 0.8$) over the cloud. Very high ratios at the higher latitude side of the cloud might be artificial. The mean intensity ratio is $R_{(2-1)/(1-0)} = 1.04$.

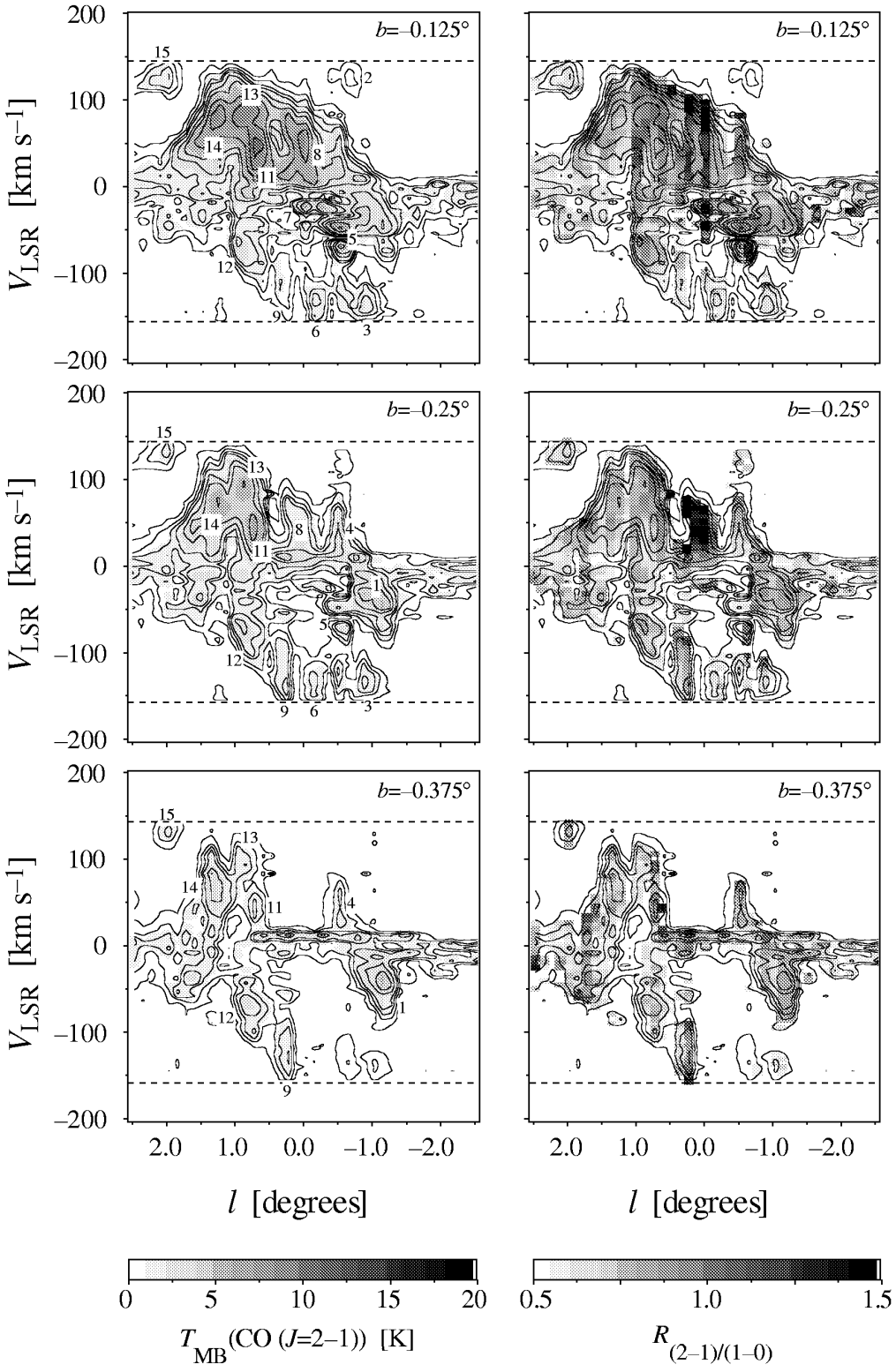

FIG. 2—*Continued*

Cloud 6 [*CO 359.9−0.1(−120)*].—This small cloud appears at $(l, b, V_{LSR}) \cong (-0.^{\circ}125, 0.^{\circ}125, -120\ \mathrm{km\ s^{-1}})$. It is a part of EMR. The intensity ratio is relatively low over the cloud, being $R_{(2-1)/(1-0)} = 0.6$–0.8. The mean intensity ratio is $R_{(2-1)/(1-0)} = 0.63$.

Cloud 7 [*CO 0.0+0.0(−20, −35)*].—This cloud is divided into two velocity components by the absorption feature at $V_{LSR} \cong -30\ \mathrm{km\ s^{-1}}$ (4.5 kpc arm). Despite the serious contamination by the foreground arm, the intensity ratio is apparently high ($R_{(2-1)/(1-0)} \geq 0.8$) over the cloud.

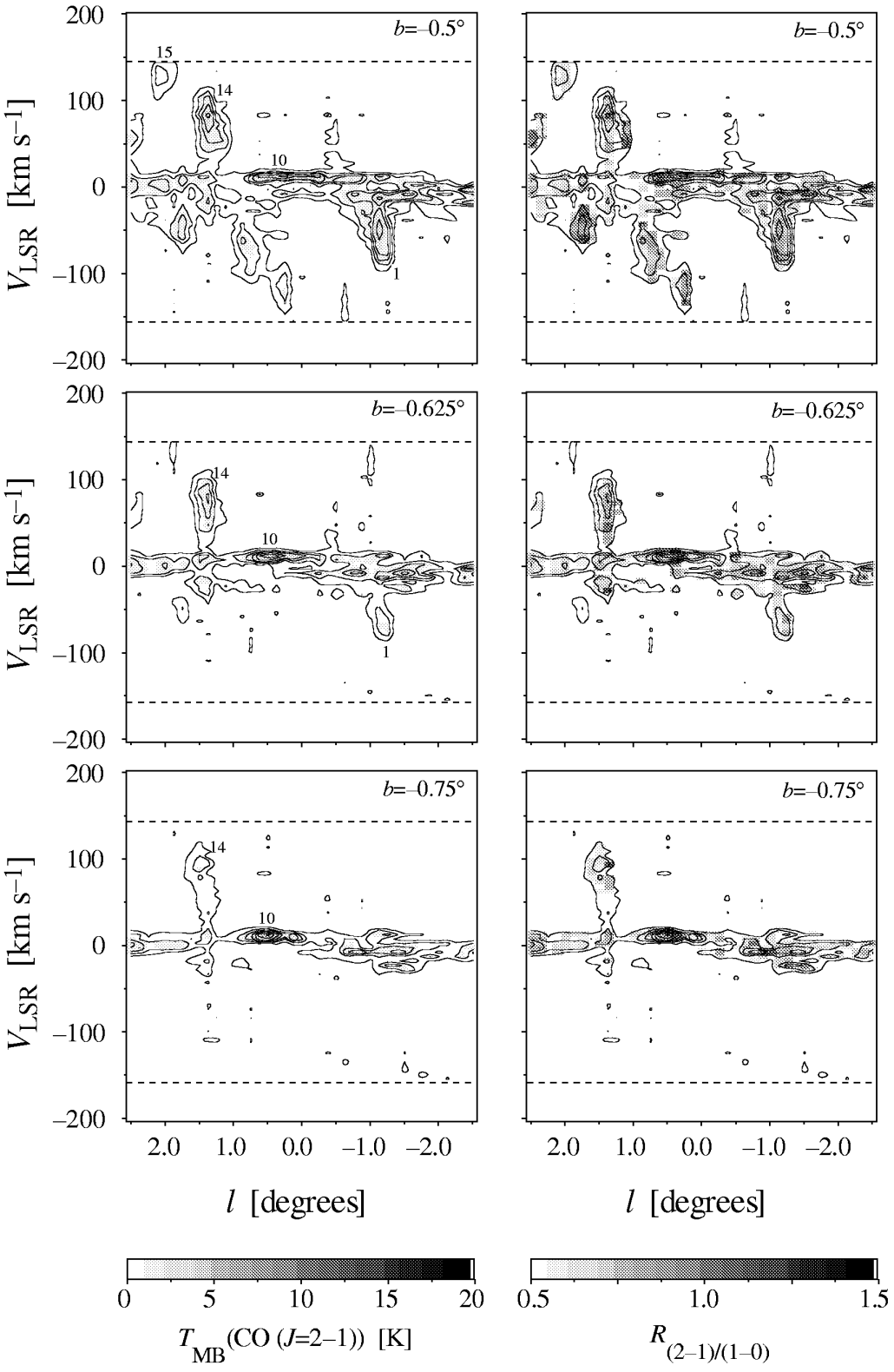

FIG. 2—*Continued*

The mean intensity ratio is $R_{(2-1)/(1-0)} = 1.12$.

Cloud 8 [*CO 0.0+0.0(+70)*].—This cloud is associated with a radio continuum source Sgr A, and hence we call it Sgr A molecular cloud complex. This appears in a wide velocity range from $V_{LSR} = 0$ km s^{-1} to 140 km s^{-1} centering at (l, b, V_{LSR}) = (0°.0, 0°.0, 70 km s^{-1}). It contains two well-known giant clouds, the +20 km s^{-1} and +40 km s^{-1} clouds, which are located close to the nucleus (e.g., Genzel

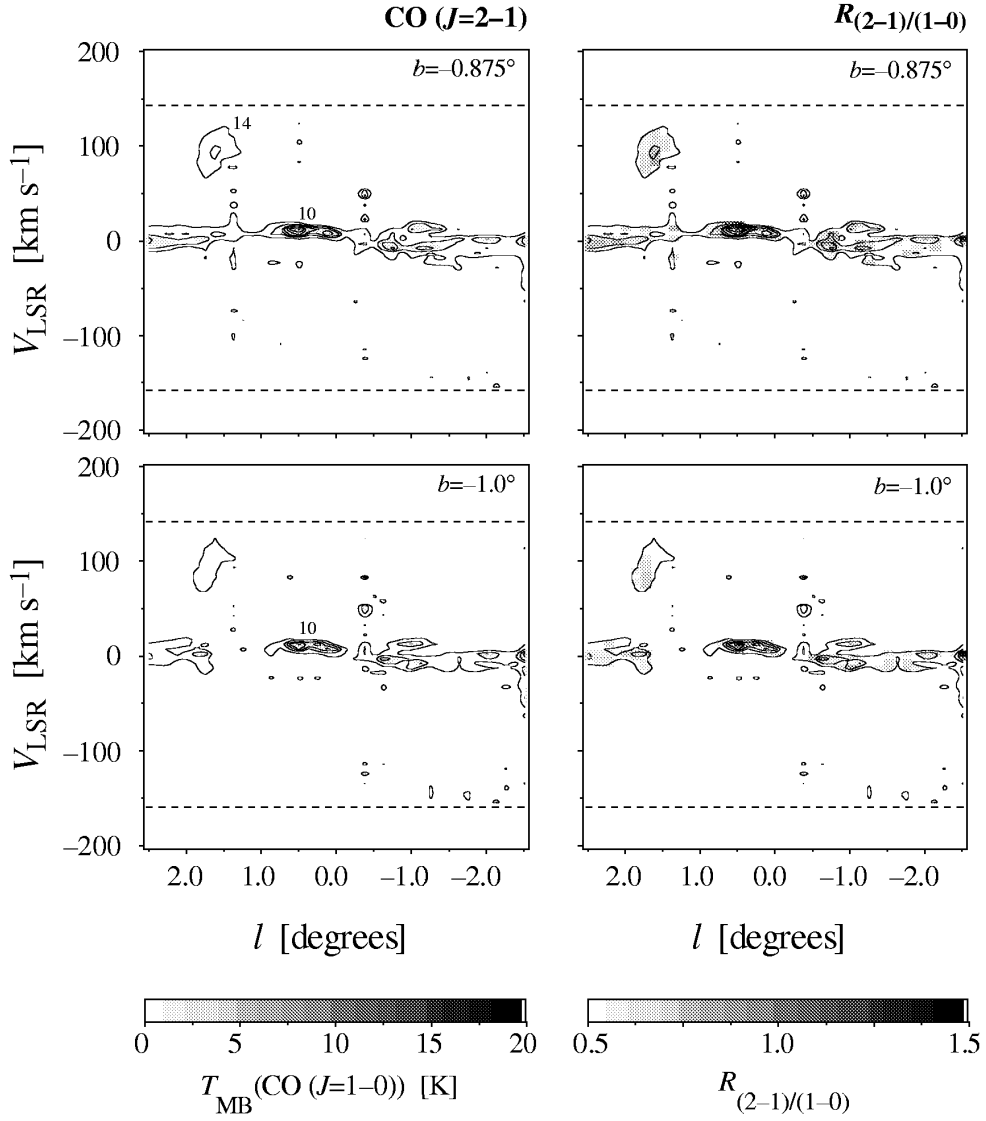

FIG. 2—*Continued*

et al. 1990). The $J = 2$–$1/J = 1$–0 intensity ratio is generally high, and it exceeds 1.2 at the cloud periphery. The mean intensity ratio is $R_{(2-1)/(1-0)} = 1.03$. At a velocity higher than $V_{LSR} = 90$ km s^{-1}, it moves away from the plane with the velocity. This higher velocity, off-plane feature is labeled independently as Cloud 8^+, which was first identified by Burton & Liszt (1983) as "inclined feature." The intensity ratio of the Cloud 8^+ is $R_{(2-1)/(1-0)} = 0.6$–0.8.

Cloud 9 [*CO 0.3−0.3*(*−130*)].—This appears at (l, b, V_{LSR}) $\cong$ (0°.25, −0°.25, −130 km s^{-1}). It is a part of EMR. The intensity ratio is $R_{(2-1)/(1-0)} = 0.6$–0.8. The mean intensity ratio is $R_{(2-1)/(1-0)} = 0.79$.

Cloud 10 [*CO 0.5−0.8*(*+20*)].—This cloud appears at (l, b, V_{LSR}) $\cong$ (0°.5, −0°.75, 20 km s^{-1}) with a narrow velocity width ($\Delta V \cong 5$ km s^{-1}). It is best seen in our data in the channel map at $V_{LSR} = 10$ to 20 km s^{-1}. Its longitudinal elongation in the l-V plane and narrow velocity width suggest that Cloud 10 is not located in the Galactic center, probably rather in the Galactic disk. The fact that H II regions associated with the Cloud 10 are observed in visible wavelength (Sharpless 1959) verifies that the cloud is in the foreground. The intensity ratio is apparently high ($R_{(2-1)/(1-0)} \geq 1.0$) near the H II regions.

Cloud 11 [*CO 0.8+0.0*(*+50*)].—This cloud is associated with the H II regions Sgr B1 at $V_{LSR} = 50$ km s^{-1} and Sgr B2 at $V_{LSR} = 64$ km s^{-1} (Pauls & Mezger 1975), and hence we call it Sgr B molecular cloud complex. This cloud centers at (l, b, V_{LSR}) = (0°.75, 0°.0, 50 km s^{-1}). The intensity ratio is $R_{(2-1)/(1-0)} = 0.7$–0.9 near the cloud center, and it exceeds unity at the cloud periphery and at higher side of the velocity. The mean intensity ratio is $R_{(2-1)/(1-0)} = 0.87$.

Cloud 12 [*CO 0.9−0.1*(*−60*)].—This cloud appears at (l, b, V_{LSR}) $\cong$ (0°.875, −0°.125, −60 km s^{-1}). It is one of the clouds which compose EMR. The intensity ratio is $R_{(2-1)/(1-0)} = 0.6$–0.8. The mean intensity ratio is $R_{(2-1)/(1-0)} = 0.77$.

Cloud 13 [*CO 0.9+0.0*(*+90*)].—This cloud centers at (l, b, V_{LSR}) = (0°.875, 0°.0, 90 km s^{-1}). Being linked with

TABLE 1

MOLECULAR CLOUDS TOWARD THE GALACTIC CENTER IDENTIFIED IN CO ($J = 2$–1) LINE

ID	Feature	l (deg)	b (deg)	V_{LSR} (km s^{-1})	Δl (deg)	Δb (deg)	S (pc)	ΔV (km s^{-1})	$T_{peak,(2-1)}$ (K)	$L_{CO(1-0)}$ (K km s^{-1} pc^2)	$L_{CO(2-1)}$	$R_{(2-1)/(1-0)}$	M_{VT} ($M_\odot$)	M_{CO} ($M_\odot$)	Identification
1	CO 358.9−0.4(−30)	−1.125	−0.375	−30	0.500	0.375	28	60	5.3	7.0E+0.5	6.0E+05	0.85	3.6E+07	3.4E+06	
2	CO 359.2+0.1(+150)	−0.750	0.125	150	0.625	0.250	25	50[a]	3.1	2.0E+05	1.4E+05	0.71	2.3E+07	9.6E+05	A part of EMR
3	CO 359.4+0.0(−120)	−0.625	0.000	−120	0.500	0.375	28	60	4.4	2.0E+05	1.7E+05	0.84	3.6E+07	9.6E+05	MC associated with Sgr C
4	CO 359.5−0.3(+30)	−0.500	−0.250	30	0.375	0.375	24	60	5.0	2.6E+05	2.1E+05	0.81	3.1E+07	1.2E+06	
5	CO 359.5+0.0(−35, −65)	−0.500	0.000	−35 −65	0.500	0.500	32	50	8.7	2.1E+05	2.2E+05	1.04	2.9E+07	1.0E+06	
6	CO 359.9−0.1(−120)	−0.125	−0.125	−120	0.375	0.125	14	60	2.4	1.5E+05	9.8E+04	0.63	1.8E+07	7.4E+05	A part of EMR
7	CO 0.0+0.0(−20, −35)[b]	0.000	0.000	−20 −35	0.250	0.250	16	40	8.2	7.3E+04	8.1E+04	1.12	9.3E+06	3.5E+05	
8	CO 0.0+0.0(+70)	0.000	0.000	70	0.625	0.250	25	110	11.6	1.1E+06	1.2E+06	1.03	1.1E+08	5.4E+06	Sgr A Molecular Cloud Complex
8+		>0.0	>0.0	$\gtrsim$ 80											"Inclined Feature"[c]
9	CO 0.3−0.3(−130)	0.250	−0.250	−130	0.250	0.375	20	80	2.4	2.5E+05	1.9E+05	0.79	4.5E+07	1.2E+06	A part of EMR
10	CO 0.5−0.8(+20)	0.500	−0.750	20	0.750	0.500	39	5	6.6	1.3E+05	1.2E+05	0.91	3.6E+05	6.4E+05	Foreground cloud
11	CO 0.8+0.0(+50)	0.750	0.000	50	0.625	0.500	36	70	10.5	1.5E+06	1.3E+06	0.87	6.4E+07	7.1E+06	Sgr B Molecular Cloud Complex
12	CO 0.9−0.1(−60)	0.875	−0.125	−60	0.500	0.625	36	50	3.4	5.6E+05	4.3E+05	0.77	3.2E+07	2.7E+06	A part of EMR
13	CO 0.9+0.0(+90)	0.875	0.000	90	0.750	0.500	39	50	11.0	1.2E+06	1.1E+06	0.96	3.6E+07	5.6E+06	
14	CO 1.4+0.0(+80)	1.375	0.000	80	0.500	0.625	36	80	10.6	2.3E+06	2.0E+06	0.85	8.3E+07	1.1E+07	
15	CO 2.0+0.0(+130)	2.000	0.000	130	0.375	0.375	24	40	2.4	1.6E+05	1.0E+05	0.64	1.4E+07	7.8E+05	A part of EMR

[a] The velocity width of CO 359.2+0.1(+150) was measured in CO ($J = 1$–0) spectra since it could not be covered by our velocity coverage.

[b] CO 0.0+0.0(−20, −35) and CO 359.5+0.0(−35, −65) are divided into two velocity components by absorption features of two foreground arms.

[c] Identified by Burton & Liszt 1983.

Cloud 11 and Cloud 14, Cloud 13 is barely identified as an individual cloud in the l-V diagrams between the latitudes $b = -0.^\circ25$ and $0.^\circ0$. The intensity ratio is $R_{(2-1)/(1-0)} =$ 0.7–0.9 near the cloud center, and it exceeds unity at the cloud periphery and at both sides of the velocity. The mean intensity ratio is $R_{(2-1)/(1-0)} = 0.96$.

Cloud 14 [*CO 1.4+0.0(+80)*].—This cloud centers at (l, b, V_{LSR}) = ($1.^\circ375$, $0.^\circ0$, 80 km s^{-1}) and appears in the channel maps between velocities +30 and +140 km s^{-1} with a large latitudinal scale height ($\Delta b \cong 0.^\circ625$). It is associated with some spurlike features sticking away from the Galactic plane at (l, b, V_{LSR}) = ($1.^\circ4$, $-0.^\circ6$, 40 km s^{-1}), ($1.^\circ4$, $0.^\circ5$, 70 km s^{-1}), and ($1.^\circ4$, $-0.^\circ7$, 90 km s^{-1}). No H II region associates with this cloud. The $J = 2$–$1/J = 1$–0 intensity ratio is $R_{(2-1)/(1-0)} = 0.7$–1.0 over the cloud, and the mean intensity ratio is $R_{(2-1)/(1-0)} = 0.85$.

Cloud 15 [*CO 2.0+0.0(+130)*].—This cloud is clearly seen in our data as a well-isolated feature centered art (l, b, V_{LSR}) = ($2.^\circ0$, $0.^\circ0$, 130 km s^{-1}). It is one of the clouds which compose the EMR. The intensity ratio is relatively low over the cloud, being $R_{(2-1)/(1-0)} = 0.5$–0.7. The mean intensity ratio is $R_{(2-1)/(1-0)} = 0.64$.

4. MOLECULAR GAS DISTRIBUTION IN THE GALACTIC CENTER

4.1. *Longitudinal Distribution*

Longitudinal distribution of CO ($J = 2$–1) (present work) and CO ($J = 1$–0) line emissions (Bitran 1987) are shown in Figure 3*a*. Molecular gas in the central few hundred parsecs of the Galaxy shows highly asymmetric longitudinal distribution with respect to the Galactic center ($l = 0°$), about two-thirds of CO emission being found on the positive longitude side (e.g., Bania 1977; Liszt & Burton 1978).

There are four prominent emission peaks in the CO ($J = 1$–0) longitudinal distribution at $l \cong -0.^\circ5$, $0.^\circ0$, $0.^\circ75$ and $1.^\circ25$. These peaks are located with a roughly regular interval of $0.^\circ6$, which corresponds to a projected distance of $\sim$90 pc. The simple linear perturbation theory of gas disk predicts that the disk will be gravitationally unstable when the system satisfies $Q \equiv \kappa c_s/2\pi G\sigma_0 < \frac{1}{2}$ (Binney & Tremaine 1987). However, using the parameter set for the Galactic center, σ_0(100–200 pc) $\cong 8.0 \times 10^2\ M_\odot\ \mathrm{pc}^{-2}$ (using the standard $N(H_2)/I_{CO}$ conversion factor), $c_s \sim \sigma_v \cong 32$ km s^{-1} (see § 4.2), and κ(150 pc) = 2.4 km s^{-1} pc^{-1} (Clemens 1985), we get $Q = 3.4$. The Q-value derived here is an underestimation because the gas surface density σ_0 is overestimated for the reason described in § 5.1. Consequently, it appears impossible for such large molecular cloud complexes to form solely by gravitational instability. This is due to large velocity shear and large velocity dispersion of the molecular cloud in the Galactic center. Other mechanisms such as collisional buildup of clouds at orbit crowdings might be required for the observed large molecular cloud complexes to grow.

4.2. *Latitudinal Distribution*

The latitudinal distributions of the $J = 2$–1 and $J = 1$–0 line emissions are shown in Figure 3*b*. These distributions show symmetrical profiles with respect to the Galactic plane, with almost the same shape in the $J = 2$–1 and $J = 1$–0 lines. The scale height of CO emission ($z_{1/e} \sim 45$ pc) is smaller than that of the stellar population ($z_{1/e} \sim 375$ pc; Blitz & Spergel 1991). Here we consider a simple plane-parallel model to estimate the z-direction velocity dispersion of the clouds (σ_z) from the observed scale heights. We assume a Gaussian-shape stellar mass distribution

$$\rho(z) = \rho_0 \exp\left(-\frac{z^2}{H^2}\right), \tag{3}$$

where H is the scale height and ρ_0 is the mass density in the midplane ($z = 0$). We do not need to consider dark matter when talking about the gravitational potential in the Galactic bulge because there is less dark matter in the bulge (Kent 1992) and it is distributed almost uniformly over the Galactic halo. The contribution of gas itself to the gravitational potential is less than 10% of the stellar contribution (see § 5), and hence it can also be neglected. Solving the Poisson

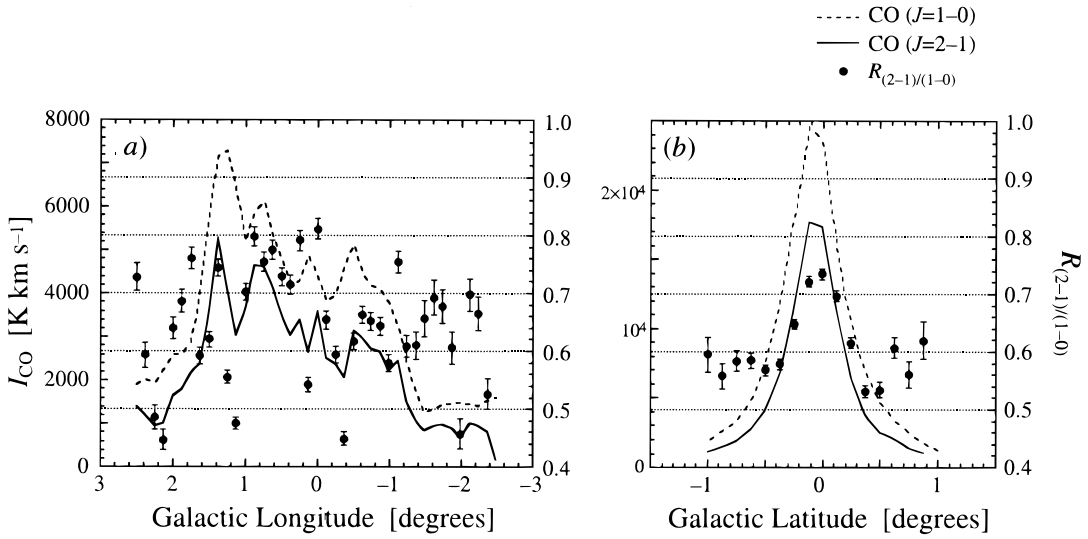

FIG. 3.—(*a*) Longitudinal distributions of CO integrated intensities and the $J = 2$–$1/J = 1$–0 intensity ratio. (*b*) Latitudinal distributions of CO integrated intensities and the $J = 2$–$1/J = 1$–0 intensity ratio. The data within the velocity range $V_{LSR} = -10$–$+20$ km s^{-1} are excluded from the calculation of the intensity ratio.

equation, $\Delta V = 4\pi G\rho$, we get the stellar gravitational potential

$$V(z) = 2\pi^{3/2} G\rho_0 H^2 F\left(\frac{z}{H}\right),$$

$$F(x) \equiv \frac{1}{\sqrt{\pi}} [\exp(-x^2) - 1] + x \operatorname{erf}(x) . \quad (4)$$

Supposing that the self-gravity of the gas layer is negligible, in the given potential $V(z)$, cloud particles with a mass m and a temperature T will have the following z-distribution in an equilibrium state:

$$n(z) = n_0 \exp\left(-\frac{mV(z)}{kT}\right)$$

$$= n_0 \exp\left(-\frac{V(z)}{\sigma_z^2}\right). \quad (5)$$

In the last reformation, we used the law of equipartition of energy, $(1/2)m\sigma_z^2 = (1/2)kT$. Note that $n(z)$ is independent of m. If we define the scale height of the molecular gas layer (H_g) as the height where $n(z)/n_0$ falls to $1/e$, the equation $V(H_g) = \sigma_z^2$ should be satisfied. The resultant expression for the σ_z is as follows:

$$\sigma_z^2 = 2\pi^{3/2} G\rho_0 H^2 F\left(\frac{H_g}{H}\right),$$

$$= 3.06 \times 10^{-2} \sigma_0(M_\odot \text{ pc}^{-2}) H(\text{pc}) F\left(\frac{H_g}{H}\right) (\text{km s}^{-1})^2 , \quad (6)$$

where σ_0 is mass surface density. Substituting $\sigma_0(200 \text{ pc}) = 1.99 \times 10^4 M_\odot \text{ pc}^{-2}$ (Oort 1977), $H = 375$ pc (Blitz & Spergel 1991), and $H_g = 45$ pc, we get $\sigma_z = 32$ km s^{-1}. The actual value for the velocity dispersion would be somewhat larger if the self-gravity of the molecular gas layer also plays a role. The z-direction velocity dispersion derived here is comparable to the typical value of the cloud-to-cloud dispersion within molecular cloud complexes ($\Delta V = \sigma_{x\text{-}y} \cong$ 30–50 km s^{-1}; Bally et al. 1988). The coincidence between σ_z estimated by the molecular scale height and observed $\sigma_{x\text{-}y}$ implies that the assumption of non–self gravitating molecular gas layer was fairly valid.

5. DYNAMICAL PROPERTIES OF THE GALACTIC CENTER MOLECULAR CLOUDS

5.1. CO *Luminosity-Virial Mass Relation and the Mass of the Galactic Center Molecular Clouds*

In general, CO luminosity of a molecular cloud scales with its virial mass. This relation found for giant molecular clouds in the Galactic disk has served as a basis of our use of the X-factor to estimate molecular mass of a region from its CO luminosity (e.g., Young & Scoville 1991). Figure 4 shows a plot of the CO luminosity versus virial mass for the molecular clouds identified in our Galactic center survey. For comparison, the disk clouds are also plotted from the data by Solomon et al. (1987). The CO luminosity ranges of identified clouds are fairly overlapped, although their ranges are different. Suprisingly, all but one cloud identified in the present work do not follow the $L_{CO} - M_{VT}$ relation of the disk clouds but appear to form a separate sequence with

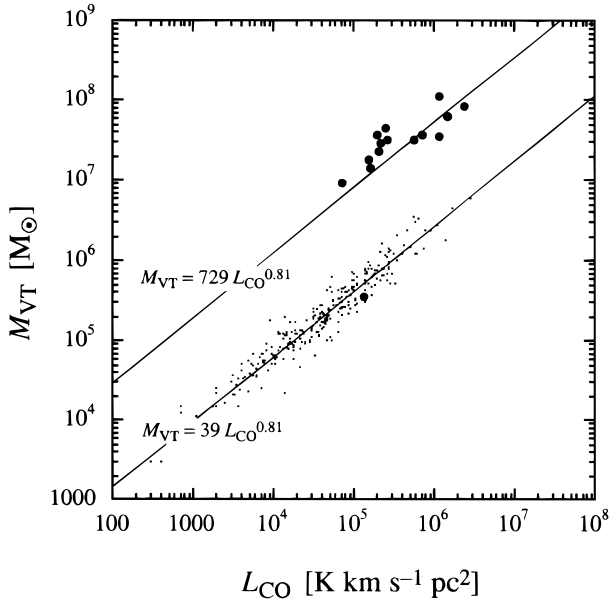

FIG. 4.—L_{CO}-M_{VT} plot for the molecular clouds identified in our survey, with the corresponding plot for the molecular clouds on the Galactic disk (Solomon et al. 1987). A cloud which is on the same trend as the disk cloud is a foreground cloud, CO 0.5−0.8(+20). Solid straight lines show the result of linear least-squares regression to the logs for the Galactic center clouds and the disk clouds.

~ 30 times larger L_{CO} for a given M_{VT}. The exception, CO 0.5−0.8(+20), is known to be a foreground disk cloud not associated with the Galactic center. The larger L_{CO}/M_{VT} ratio found in the Galactic center molecular clouds leads to the sharp discrepancy between the virial mass and the CO luminosity mass estimated with the standard X-factor calibrated for the disk clouds as we see in Table 1. Figure 5*a* illustrates the situation, i.e., the virial masses are larger than the mass derived from L_{CO} and the standard X-factor by at least 1 order of magnitude.

It is impossible to solve this M_{CO}-M_{VT} discrepancy for the Galactic center molecular clouds by introducing a large X-factor (~ 10 times of the standard value) since observations of γ-ray emission (Blitz et al. 1985) and far-infrared emission (Cox & Laureijs 1989) suggest that the X-factor in the Galactic center is smaller than that in the solar neighborhood ($\sim \frac{1}{5}$ of the standard value).

This discrepancy can naturally be solved if we notice that the Galactic center molecular clouds may not be bound by their self-gravity. Rather, they may be in equilibrium with the high external pressure in the Galactic center environment (Spergel & Blitz 1992). The pressure we mean is not only the microscopic thermal pressure ($nT_k \sim$ several $\times 10^3$ cm^{-3} K for disk clouds) but also includes the pressure by macroscopic turbulence within the interstellar medium. Since the macroscopic turbulent pressure is communicated to individual clouds also via magnetic fields, cloud-cloud, and cloud-intercloud interactions, it can be considerably larger than the microscopic thermal pressure. We can write the virial theorem in the presence of external pressure p as

$$3M_{VT}\sigma_v^2 - \frac{GM_{VT}^2}{R_e} = 4\pi R_e^3 p , \quad (7)$$

where R_e is the effective radius defined by $f_p S$. This equation gives two solutions for the equilibrium mass for a given set

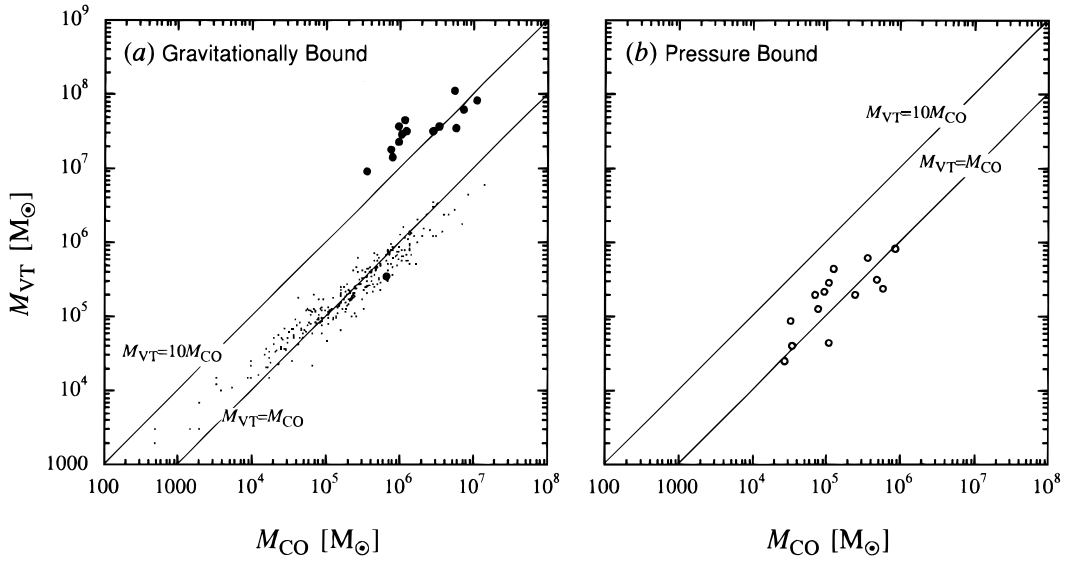

FIG. 5.—(*a*) M_{CO}-M_{VT} plot for the molecular clouds identified in our survey with the correponding plot for the molecular clouds on the Galactic disk (Solomon et al. 1987). (*b*) M_{CO}-M_{VT} plot for the molecular clouds in the Galactic center, excluding a foreground cloud CO 0.5−0.8(+20), using the formula for pressure-bound clouds ($p/k = 3 \times 10^5$ cm^{-3} K).

of size and velocity dispersion, when the condition $p < p_0 \equiv 9\sigma_v^4/(16\pi R_e^2 G)$ is satisfied.

The value p_0 is proportional to a fourth power of the size–line width coefficient ($\sigma_v/S^{0.5}$). A dimensionless parameter $\beta \equiv p/p_0$ is expressed by three dynamical parameters as $(|U|/T) \times (P/T)$, where $U = -GM_{VT}^2/R_e$ (gravitational potential energy), $T = (3/2)\ M_{VT}\,\sigma_v^2$ (internal kinetic energy), and $P = 4\pi R_e^3\, p$ (energy of external pressure). We have two equilibrium masses expressed as follows:

$$M_{VT} = \alpha_\pm M_0\ ,$$
$$\alpha_\pm = \tfrac{1}{2}(1 \pm \sqrt{1-\beta})\ (+: \text{Gravitationally bound};\ -: \text{Pressure bound})\ , \quad (8)$$

where $M_0 = 3R_e\sigma_v^2/G$—virial mass for gravitationally bound cloud with no external pressure ($p = 0$). We can simplify the solutions in case of $\beta \ll 1$ (this condition is satisfied for the Galactic center molecular clouds; see Table 2) as follows:

$$M_{VT} \cong \left(1 - \frac{\beta}{4}\right) M_0 \equiv M_{VT}(g)\ \text{(gravitationally bound)}\ ,$$

or

$$M_{VT} \cong \frac{\beta}{4}\, M_0 \equiv M_{VT}(p)\ \text{(pressure bound)}\ . \quad (9)$$

We note in equation (8) that the gravitationally bound solution varies from M_0 within a factor of 2, while the pressure bound solution varies over orders of magnitude. This means that the gravitationally bound solution cannot explain the observed large discrepancy in L_{CO}-M_{VT} relation. We take the pressure bound solution as an equilibrium mass in the following discussion.

Here we can redefine the X-factor for pressure bound clouds following the discussion by Young & Scoville (1991). For an opaque molecular cloud with uniform CO bright-

TABLE 2

MASSES OF THE GALACTIC CENTER MOLECULAR CLOUDS

ID	Feature	$M_{VT}(g)$ ($M_\odot$)	$M_{CO}(g)$ ($M_\odot$)	$\beta/4$[a]	$M_{VT}(p)$ ($M_\odot$)	$M_{CO}(p)$ ($M_\odot$)
1.....	CO 358.9−0.4(−30)	3.6E+07	3.4E+06	5.5E−03	2.0E+05	2.5E+05
2.....	CO 359.2+0.1(+150)	2.3E+07	9.6E+05	9.5E−03	2.2E+05	9.4E+04
3.....	CO 359.4+0.0(−120)	3.6E+07	9.6E+05	5.5E−03	2.0E+05	7.1E+04
4.....	CO 359.5−0.2(+30)	3.1E+07	1.2E+06	4.1E−03	1.3E+05	7.9E+04
5.....	CO 359.5+0.0(−35, −65)	2.9E+07	1.0E+06	1.5E−02	4.4E+05	1.3E+05
6.....	CO 359.9−0.1(−120)	1.8E+07	7.4E+05	1.4E−03	2.5E+04	2.7E+04
7.....	CO 0.0+0.0(−20, −35)	9.3E+06	3.5E+05	9.3E−03	8.7E+04	3.4E+04
8.....	CO 0.0+0.0(+70)	1.1E+08	5.4E+06	4.1E−04	4.5E+04	1.1E+05
9.....	CO 0.3−0.3(−130)	4.5E+07	1.2E+06	8.7E−04	4.0E+04	3.5E+04
11.....	CO 0.8+0.0(+50)	6.4E+07	7.1E+06	5.0E−03	3.2E+05	5.0E+05
12.....	CO 0.9−0.1(−60)	3.2E+07	2.7E+06	1.9E−02	6.2E+05	3.7E+05
13.....	CO 0.9+0.0(+90)	3.6E+07	5.6E+06	2.3E−02	8.1E+05	8.5E+05
14.....	CO 1.4+0.0(+80)	8.3E+07	1.1E+07	2.9E−03	2.4E+05	6.0E+05
15.....	CO 2.0+0.0(+130)	1.4E+07	7.8E+05	2.1E−02	2.9E+05	1.1E+05

[a] β are calculated with the pressure $p/k = 3 \times 10^5$ cm^{-3} K.

ness, total CO luminosity can be expressed as $L_{CO} = 2\pi R_e^2 T_{CO}\,\sigma_V$. Taking the pressure bound solution $M_{TV}(p) = (\beta/4)M_0$ as cloud mass and equating this to $(4/3)\pi R_e^3\,\rho$ (ρ is the mean mass density), the relation between the cloud mass $[M_{CO}(p)]$ and the total CO luminosity (L_{CO}) becomes

$$M_{CO}(p) = \left(\frac{\beta}{4}\right)^{1/2}\left[\left(\frac{\rho}{\pi G}\right)^{1/2}\frac{1}{T_{CO}}\right]L_{CO}$$
$$= 1.6\times 10^{-20}\left(\frac{\beta}{4}\right)^{1/2} X_0\,L_{CO}\ (\mathrm{K\ km\ s^{-1}\ pc^2})\,. \quad (10)$$

This means that, even for pressure bound clouds, the total CO luminosity scales with the total mass of molecular clouds to the extent that the ratio $(\beta\rho)^{1/2}/T_{CO}$ does not vary among clouds and the CO emission from separate clouds along each line of sight does not overlap in velocity. In addition, the equation means that the X-factor for pressure-bound clouds becomes $(\beta/4)^{1/2}X_0$ (where X_0 is the X-factor for a purely gravitationally bound cloud in an absence of the external pressure) when $\beta \ll 1$ is satisfied. The value of the $(\beta/4)$ ranges from 10^{-4} to 10^{-2} for the Galactic center molecular clouds (see Table 2). These small values of β are due to small U/T, which indicates an almost pure pressure equilibrium case for the molecular clouds in the Galactic center.

The different β-dependencies of $M_{VT}(\propto\beta)$ and M_{CO} $(\propto\beta^{1/2})$ for pressure-bound clouds enable us to fit the observed L_{CO}-M_{VT} relation for the Galactic center molecular clouds to $M_{VT} = M_{CO}$ line by varying external pressure p. Taking the standard X-factor in the Galactic disk $(=3.0\times 10^{20}\ \mathrm{cm^{-2}[K\ km\ s^{-1}]^{-1}})$ as X_0, and excepting for the foreground cloud CO $0.5-0.8(+20)$, we get the best agreement between the M_{VT} and M_{CO} with $p/k = 3\times 10^5$ $\mathrm{cm^{-3}\ K}$ (Fig. 5*b*; Table 2). This pressure is 1 order of magnitude higher than the thermal pressure in the solar vicinity, but about 1 order of magnitude lower than the thermal pressure estimated for the hot gas in the Galactic center observed in X-ray emission, $p_{hot}/k = (3\text{–}6)\times 10^6\ \mathrm{cm^{-3}\ K}$ (Yamauchi et al. 1990). The disagreement between the macroscopic external pressure we expect and the observed pressure of the hot gas seems not to be so serious because the electron density n_e estimated from the X-ray emission is based on the emission measure $n_e^2\,L$ and is naturally biased to the denser region with a higher pressure. Considering the equipartition of energy, the magnetic field pressure there would be similar to those of hot gas and molecular clouds in this region. We conclude that the Galactic center molecular clouds larger than $\sim$30 pc are in equilibrium with the macrocopic external pressure from hot gas and/or magnetic field. Simple virial equilibrium analyses would result in a gross overestimate of the masses of the Galactic center molecular clouds.

Using the X-factor redefined for pressure bound clouds, $\alpha_- X_0 \cong (\beta/4)^{1/2}X_0 = 0.24\times 10^{20}\ \mathrm{cm^{-2}\ (K\ km\ s^{-1})^{-1}}$, the total molecular mass within the inner 400 pc of the Galaxy becomes $M_g \cong 2\times 10^7\ M_\odot$. This estimate is a lower limit to the actual mass for the following two reasons. First, smaller scale dense substructures in the clouds or cloud complexes could be gravitationally bound, which might give some addition to the total molecular mass estimated by pressure-bound equilibrium. Second, in case that disk clouds are also in pressure-bound equilibrium, the equation $\alpha_- X_0 = 3.0\times 10^{20}\ \mathrm{cm^{-2}\ (K\ km\ s^{-1})^{-1}}$ gives larger X_0, and thereby results in larger β because $\beta\propto(X_0\,L_{CO}/M_0)^2$ by equations (9) and (10). both of these changes raise the total molecular mass estimation by pressure-bound equilibrium.

Our estimate, $M_g \gtrsim 2\times 10^7\ M_\odot$, is compatible with the upper limit to the total gas mass of $6\times 10^7\ M_\odot$ derived from γ-ray observations (Blitz et al. 1985). The total gas mass within the central 400 pc of the Galaxy may be $M(H_2) = (2\text{–}6)\times 10^7\ M_\odot$. Our estimate is also consistent with the mass estimate from $C^{18}O$ $(J = 1\text{–}0)$ line observations, $M(H_2)\cong(3^{+2}_{-1})\times 10^7\ M_\odot$ (Dahmen et al. 1996). Corresponding star formation efficiency (SFE $\equiv$ SFR/M_g) is of the same order of magnitude as that in the molecular ring at $R = 4\text{–}6$ kpc in the Galaxy.

5.2. *Size–Line Width Relation*

Figure 6 shows that the size–line width relation of the Galactic center molecular clouds in comparison with that of the GMCs in the Galactic disk. The clouds in the Galactic center have line widths larger than those of disk clouds with similar sizes. If we assume that the Galactic center clouds obey the same power law with an index of 0.5 as the disk clouds do, a linear least-squares fit gives a result $\sigma_V = (5.0\pm 0.5)S^{0.5}$, where σ_V is in km s^{-1} and S is in parsecs. The size–line width coefficient of the Galactic center clouds is a factor of 5 larger than that of molecular clouds in the Galactic disk, $\sigma_V = (1.0\pm 0.1)S^{0.5\pm 0.05}$ (Solomon et al. 1987).

Attempts have been made to understand the size–line width relation (S-σ_V relation) for disk clouds in terms of model clouds in pressure equilibrium with the intercloud medium (Chiéze 1987; Maloney 1988). According to these models, the size–line width coefficient $(\sigma_V/S^{0.5})$ varies with a $\frac{1}{4}$ power of exernal pressure. The large size–line width coefficient in the Galactic center can barely be explained in this term if the pressure there is about 3 orders of magnitude larger than that in the Galactic disk. A polytropic cloud under external pressure by Elmegreen (1989) implies that

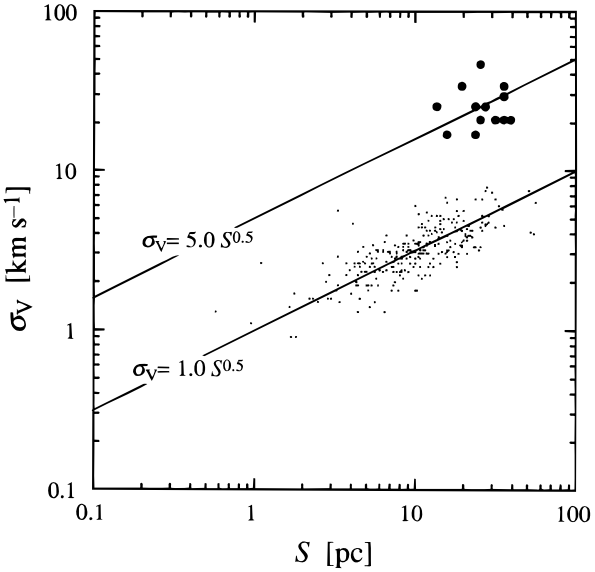

FIG. 6.—Size-velocity line width plot for the molecular clouds in the Galactic center, excluding a foreground cloud CO $0.5-0.8(+20)$, with the corresponding plot for the molecular clouds in the Galactic disk (Solomon et al. 1987). Solid straight lines show the results of linear least-squares regression to the logs for the Galactic center clouds and the disk clouds.

the external pressure 1 order of magnitude higher than that in the Galactic disk leads to the size–line width coefficient a factor of 5 larger, which is consistent with the observations. The above cloud models assume a self-gravitating cloud with external pressure. They may not be applied to molecular clouds in the Galactic center, which are almost purely in pressure equilibrium (see § 5.1).

High external pressure and/or highly turbulent environment in the Galactic center region must be responsible for the high value of size–line width coefficient. A simple formalization standing on purely pressure equilibrium cloud model would be essential to clarify the physics which determine the size–line width relation of molecular clouds.

5.3. *Implications to Molecular Clouds in the Galactic Disk and the Other Galaxies*

Our conclusions in § 5.1 points out the possibility that even some giant molecular clouds in the Galactic disk and other galaxies could not be gravitationally bound but in equilibrium with external pressure. If so, their masses must be at least a factor of 2 lower than that estimated from simple virial analysis (see eq. [8]). Recent γ-ray observations with EGRET toward Orion region implies a low X-factor, $X = (1.06 \pm 0.14) \times 10^{20}$ cm^{-2} (K km s^{-1})$^{-1}$ (Digel, Hunter, & Mukherjee 1995), which leads to a mass a factor of 3 lower than that estimated from simple virial analysis.

Figure 7 shows L_{CO}-M_{VT} plots of the molecular clouds in the Galaxy and in some other galaxies (LMC: Cohen et al. 1988; SMC: Rubio, Lequeux, & Boulanger 1993; M31: Vogel, Boulanger, & Ball 1987; M33:Wilson & Scoville 1990; IC 10: Wilson & Reid 1991). Here again, M_{VT} is the virial mass for the gravitationally bound cloud with no external pressure ($=M_0$). In LMC and SMC, clouds or cloud complexes show the proportionality between L_{CO} and M_{VT}. However, the proportional coefficient, M_{VT}/L_{CO}, varies from a galaxy to another; it ranges over 2 orders of magnitude. Although a lower metallicity can explain a higher M_{VT}/L_{CO} to some degree, for instance, LMC (Cohen et al. 1988) and SMC (Rubio et al. 1991, 1993), the difference in metallicity cannot explain the discrepancy between the Galactic disk and the Galactic center. The dependence of M_{VT}/L_{CO} on metallicity appears to be not as straightforward as proposed even for LMC and SMC clouds (Rubio 1997).

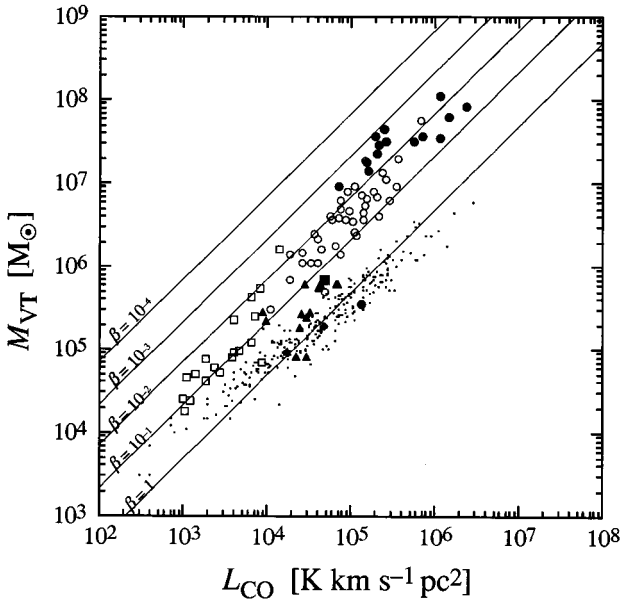

FIG. 7.—L_{CO}-M_{VT} plots for the molecular clouds in the Galaxy (*dots*, Galactic disk; *filled circles*, Galactic center) and some extragalaxies (*open circles*, LMC; *open rectangles*, SMC; *filled diamonds*, M31; *filled triangles*, M33; *filled rectangle*, IC 10) with the model lines at the various values of β (see the context in § 5.1 for the definition).

The large variation in M_{VT}/L_{CO} suggests an interesting possibility that the clouds in these galaxies are also in pressure equilibrium rather than self-gravitating. The pressure equilibrium solution in equation (8) can explain the large variations of M_{VT}/L_{CO} without any unplausible assumption. If we know both of M_{VT}/L_{CO} and size–line width coefficient of the clouds in a region, we can estimate the equilibrium pressure and the actual X-factor using the method described in § 5.1. It might be meaningful to see the correlation of the equilibrium pressure with those of X-ray–emitting hot gas or magnetic field.

Concentrations of molecular gas has been observed toward central regions of many galaxies. They are quite luminous in CO, and, when scaled with the "standard" X-factor calibrated for the disk clouds in the Galaxy, their mass amounts to a significant fraction of the total mass in the central a few hundred parsec regions (e.g., Young & Scoville 1991; Henkel, Baan, & Mauersberger 1991). The case for pressure-bound equilibrium of Galactic center molecular clouds presented in this paper raises an alarm: we might be heavily overestimating the mass of these nuclear molecular condensations.

6. THE $J = 2$–$1/J = 1$–0 INTENSITY RATIO

In this section, we analyze the $J = 2$–$1/J = 1$–0 intensity ratios of the CO emission from the Galactic center molecular clouds in comparison with those of the molecular clouds in the Galactic disk. For a reference, we first summarize the current knowledge of the CO $J = 2$–$1/J = 1$–0 ratios of the disk clouds before we attempt to understand the meanings of the ratios exhibited by the Galactic center molecular clouds.

6.1. *Molecular Gas in the Galactic Disk*

With the 60 cm telescope, we have made unbiased Galactic plane surveys as well as detailed observations of typical molecular clouds in the solar vicinity. The latter include mapping of the Orion A and B giant molecular clouds (Sakamoto et al. 1994), the Taurus dark cloud (Hayashi et al. 1996), and the Rosette molecular cloud (Morino et al. 1996). The results are summarized as follows (see also Hasegawa 1996).

The CO $J = 2$–$1/J = 1$–0 ratio [$R_{(2-1)/(1-0)} \equiv I_{CO(2-1)}/I_{CO(1-0)}$] varies from place to place in each cloud and from one cloud to another. The total $J = 2$–$1/J = 1$–0 luminosity ratios for these molecular clouds vary from 0.53 ± 0.01 in Taurus molecular cloud to 0.75 ± 0.01 in Orion A molecular cloud. Figure 8 shows the intensity ratio spectra, the fractional distribution of the CO ($J = 1$–0) intensity with $R_{(2-1)/(1-0)}$, for two representative molecular clouds in the solar neighborhood and the Galactic center molecular clouds. Since CO ($J = 1$–0) intensity is roughly proportional to the total molecular mass (see § 5.1), these ratio spectra show molecular mass fraction at certain condition indicated by $R_{(2-1)/(1-0)}$. The ratio spectra for Taurus and Orion molecular clouds show a clear difference: in the

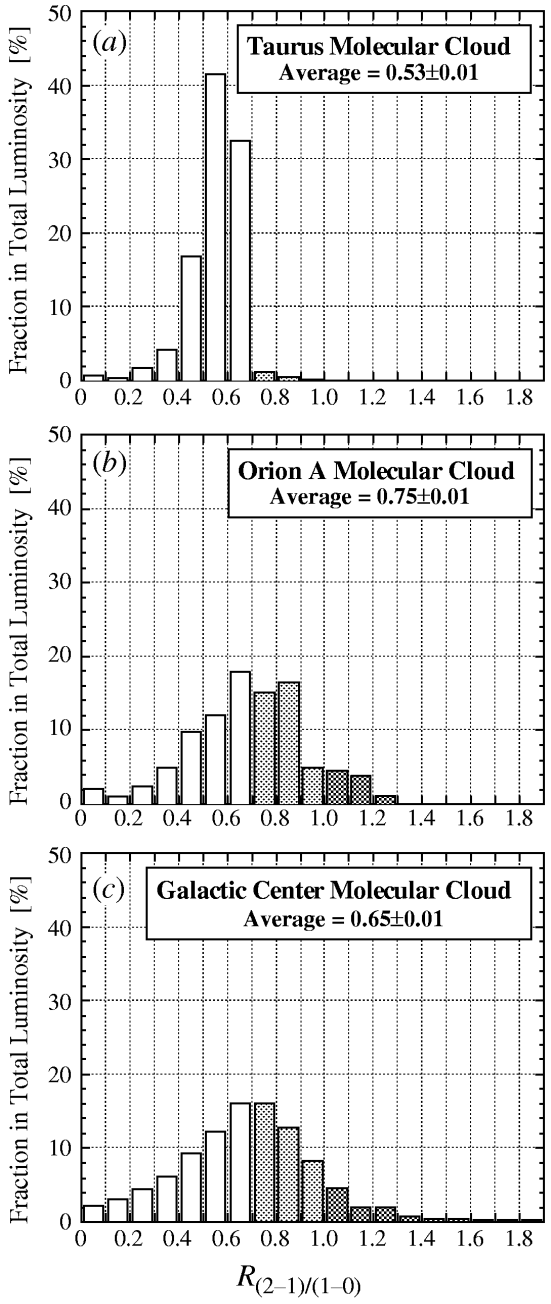

FIG. 8.—Intensity ratio spectra, the fractional distribution of the CO ($J = 1$–0) intensity with $R_{(2-1)/(1-0)}$, for (*a*) Taurus molecular cloud, (*b*) Rosette molecular cloud, and (*c*) the Galactic center molecular cloud complex. Data integrated over the full velocity width were used for Taurus and Orion molecular clouds, spectrum data binned every 5 km s^{-1} velocity width were used for the Galactic center molecular cloud complex. Gases with low ratio (LRG, *white*), high ratio (HRG, *light gray*), and very high ratio (VHRG, *dark gray*) explained in the text are shown by gray scales.

Taurus dark cloud, most emission comes from the gas with the ratio $R_{(2-1)/(1-0)} < 0.7$. We call it "low ratio gas" (LRG). In Orion A giant molecular cloud, on the other hand, a significant fraction of the luminosity comes from the gas with $R_{(2-1)/(1-0)} = 0.7$–1.0 and that with $R_{(2-1)/(1-0)} > 1.0$. We call them "high ratio gas" (HRG) and "very high ratio gas" (VHRG), respectively. This is a common characteristic of giant molecular clouds with high mass star formation (Sakamoto et al. 1994; Morino et al. 1996).

The unbiased surveys of the Milky Way have shown that $R_{(2-1)/(1-0)}$ increases from 0.6 in the solar neighborhood to 0.75 at 4 kpc from the Galactic center ("Galactic trend"; Handa et al. 1993; Sakamoto et al. 1995; Sorai et al. 1996). This trend can be understood in terms of the increased contribution of HRG that concentrates in the spiral arms in the inner Galaxy.

The increase in the ratio from LRG to HRG reflects a variation of the excitation condition at "CO photospheres," where most of the photons escaping from the cloud are emitted (see § A3. The excitation condition there is connected to hydrogen density and temperature near and inside the photospheres. A simple one-zone analysis based on the large velocity gradient approximation supports this idea (see Appendix). VHRG is often observed toward molecular gas within $\sim$15 pc from adjacent H II regions (Morino et al. 1996). This is a manifestation of the optically thin dense and warm layer of gas that envelopes the clouds or their subcondensations (Castets et al. 1990; Gierens, Stuzki, & Winnewisser 1992).

6.2. *Overall Properties of Molecular Gas in the Galactic Center*

Dependencies of the $J = 2$–$1/J = 1$–0 intensity ratio on the galactic longitude and latitude are presented in Figure 3. The emission within the velocity range $V_{LSR} = -10$ to $+20$ km s^{-1} is excluded from the analysis since it is severely absorbed by foreground gas in the Galactic disk. While molecular gas in the midplane high-intensity ratio [$R_{(2-1)/(1-0)} \cong 0.74$], molecular gas at $|b| \geq 0.^{\circ}25$ exhibits low intensity ratio [$R_{(2-1)/(1-0)} \cong 0.6$]. The trend is mainly due to the systematic decrease of relative HRG fraction with distance from the Galactic plane (Fig. 9), as is the case for the "Galactic trend" (see § 6.1). Along the Galactic longitude, the intensity ratio fluctuates without a clear trend. This fluctuation is due to the existence of some large molecular cloud complexes with high ratio [$R_{(2-1)/(1-0)} = 0.8$–1.0] in the Galactic plane. $R_{(2-1)/(1-0)}$ weakly peaks at $l = 0^{\circ}$, where an extraordinary high abundance of VHRG was observed (see the next section).

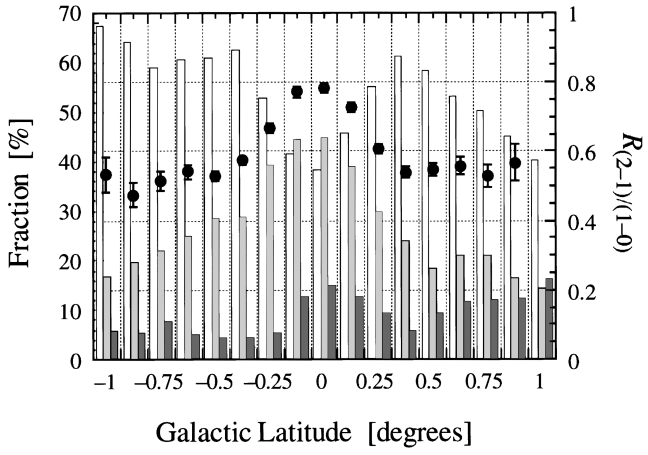

FIG. 9.—Relative fraction of low ratio gas (LRG, *white*), high ratio gas (HRG, *light gray*), and very high ratio gas (VHRG, *dark gray*) along the galactic latitude with the average $R_{(2-1)/(1-0)}$ (*filled circles*).

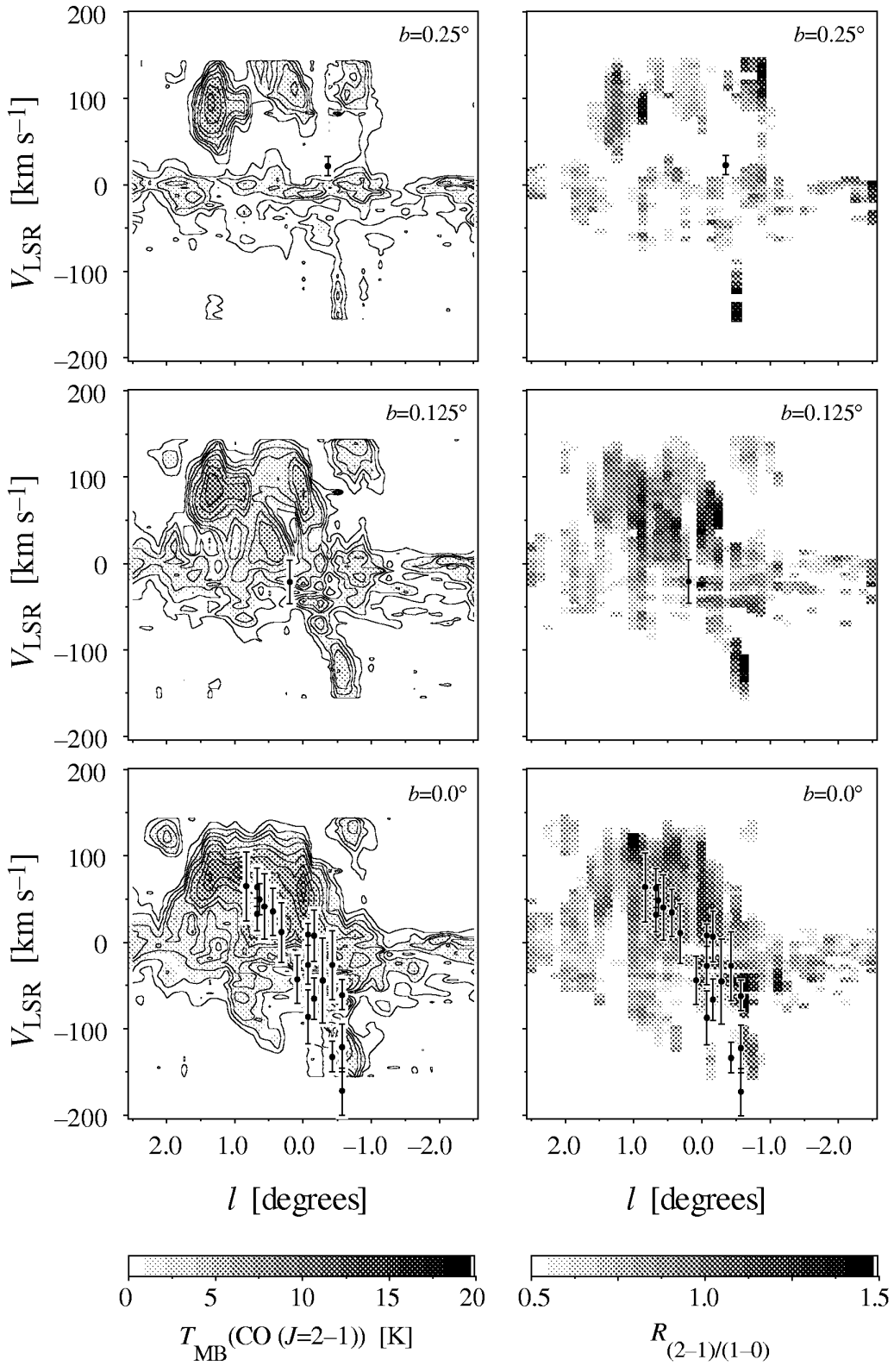

FIG. 10.—Longitude-velocity diagrams (l-V diagrams) of H109α hydrogen recombination line (Pauls & Mezger 1975) superposed on that of CO (J = 2–1) line emission and the J = 2–1/J = 1–0 intensity ratio. Contours of CO (J = 2–1) line temperature are drawn as same as Fig. 2. The intensity ratio is calculated in the region where the CO (J = 1–0) line mean main-beam temperature exceeds 2 K.

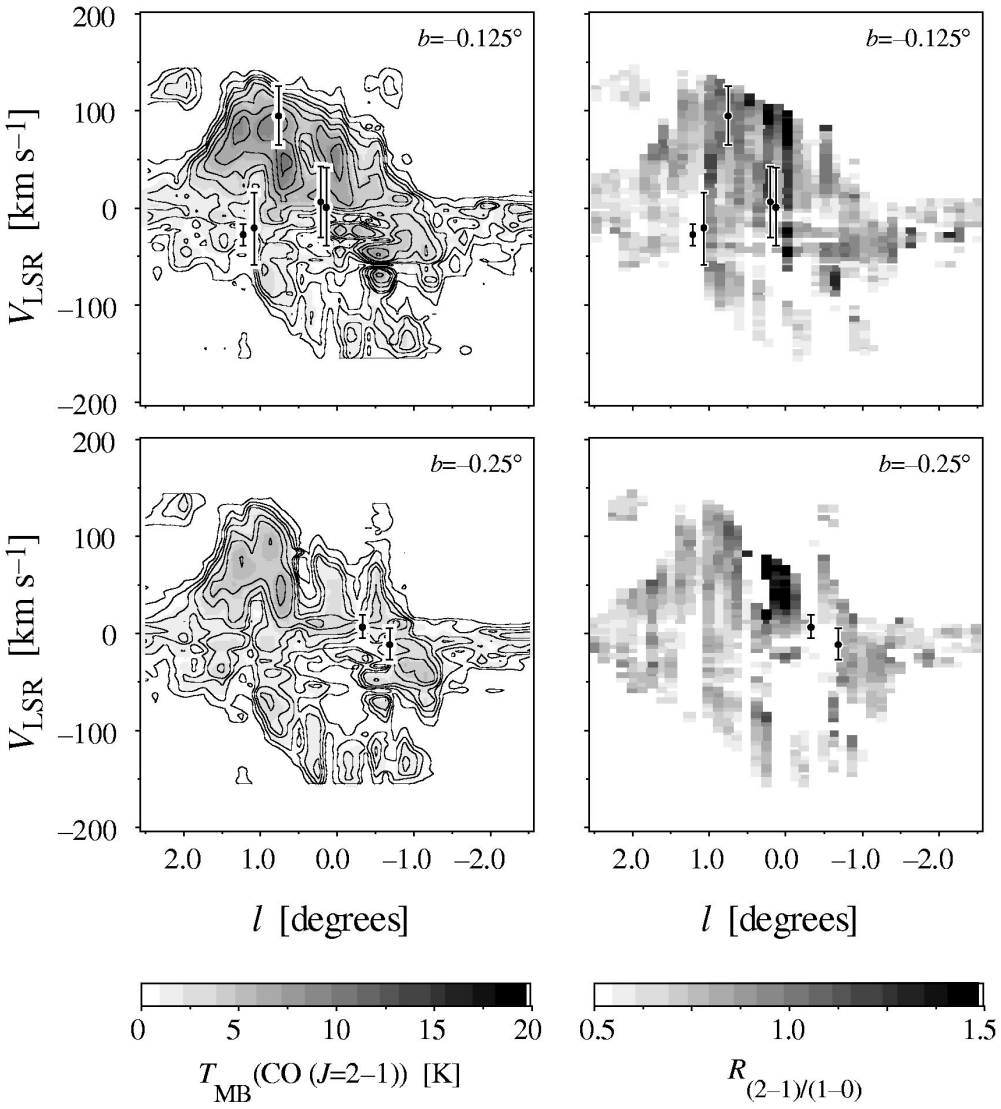

FIG. 10—*Continued*

Figure 10 shows the *l*-*V* diagrams of the intensity ratio together with the distribution of H II regions observed in hydrogen recombination lines (Pauls & Mezger 1975). The kinematics of these H II regions is described as a rotating ringlike region of active star formation with a radius of ~ 100 pc (star-forming ring; see Paper I). The molecular gas associated with the ring exhibits ratios in the range of 0.7–1.0, which suggest relatively high densities at CO photospheres. This agrees with its morphology with steep edges found by high-resolution mapping with the NRO 45 m telescope (Oka et al. 1996b).

Although gas with very high ratios [$R_{(2-1)/(1-0)} \geq 1.0$] appears in a longitude range similar to the star-forming ring, it is shifted in velocity by ~ 50 km s^{-1} (Paper I). A close examination of the velocity channel maps of the intensity ratio (Fig. 1) shows that the VHRG exists in the outskirts of clouds in position and velocity. This small-scale anticorrelation between H II regions and the gas with very high ratios argues against the possibility of the emission arising from dense photodissociation regions associated with the H II regions. We tentatively assign this very high ratio component to less dense fluffy clouds in the outskirts of the star-forming ring exposed to intense UV radiation from the ring. In these clouds, the density gradient across the CO photospheres is shallower and the gas temperature there is higher, so that the $J = 2$–1 photosphere would be significantly larger than that for $J = 1$–0. A larger $J = 2$–1/$J = 1$–0 ratio may follow as a result of a larger beam-filling factor in the $J = 2$–1 line relative to the $J = 1$–0 and/or a line brightness higher in $J = 2$–1 than in $J = 1$–0 due to a temperature gradient near cloud surfaces.

The total luminosity ratio between $J = 1$–0 and $J = 2$–1 line is $R_{(2-1)/(1-0)} = 0.64 \pm 0.01$ when we integrate the emission over $|b| \geq 1°$, $-2.°5 \leq l \leq 2.°5$, and $|V_{LSR}| \leq 150$ km s^{-1}. The error quoted is mainly due to baseline uncertainty of $J = 2$–1 line and does not include errors in antenna efficiencies. Errors in antenna efficiencies of the both telescopes do not change the trend of the ratio, although they shift its

absolute values. A part of the CO emission in this integration range comes from local molecular gas, and we have removed such local emission or absorption features to get the total luminosity ratio. However, the subtraction of foreground emission/absorption did not alter the total intensity ratio at all because its contribution is small ($\lesssim 20\%$ in the $J = 1$–0 line) and the foreground gas exhibits similar ratios. Figure 8*c* shows the ratio spectrum for the Galactic center molecular cloud complex for the data binned every 5 km s^{-1} velocity width. The ratio spectrum peaks at $R_{(2-1)/(1-0)} \cong 0.7$, which is a little higher than that of the molecular clouds in the solar neighborhood (Figure 8*a*, *b*). The relative fraction of HRG and VHRG is not particularly high compared with the gas in the Galactic disk.

The observed $J = 2$–$1/J = 1$–0 luminosity ratio indicates that the total CO emission from the Galactic center is dominated by the emission from low-density [$n(H_2) \cong 10^{2.5}$ cm^{-3}] gas. In addition, high gas kinetic temperature in this region suggested by NH_3 inversion line ratios ($T_k = 30$–60 K; Morris et al. 1983) reduces the density by the intensity ratio because of the two effects discussed in the Appendix A3. In this sense, the average density derived by the total luminosity ratio on the basis of one-zone analysis is an upper limit to the density in CO photospheres.

The low density in the Galactic center molecular clouds is also implied by the CO ($J = 1$–0)–CO ($J = 2$–1) intensity correlation plot (Fig. 11). The main ridge of the intensity correlation shows rough straight line with a slight bend near the origin. This trend can be reproduced by the large velocity gradient model with $n(H_2) = 10^2$ cm^{-3} and a surface filling factor of 0.33 as shown by the curves. Each curve represents a sequence of the total gas column density with the other parameter fixed. The good fit also implies that one-zone assumption between $J = 1$–0 and $J = 2$–1 lines would be approximately valid for a majority of the data points. Any model curves at higher density [$n(H_2) \geq 10^3$ cm^{-3}] cannot reproduce the observed data. The emission from diffuse clouds with shallow temperature gradient at their surfaces dominates the total CO luminosities from the Galactic center.

The density derived here [$n(H_2) \lesssim 10^{2.5}$ cm^{-3}] seems to be inconsistent with the results from CS, NH_3, and HCN observations, which suggest high-density [$n(H_2) \gtrsim 10^4$ cm^{-3}] gas prevails over the Galactic center region. This inconsistency is solved by introducing the two emission components, which are low-density [$n(H_2) \lesssim 10^3$ cm^{-3}] "diffuse" clouds with beam filling factor of ~ 1 and high-density [$n(H_2) \gtrsim 10^4$ cm^{-3}] "clumps" with small beam filling factor, to the Galactic center molecular clouds. In this situation, CO emission mainly traces diffuse clouds, while CS, NH_3, and HCN emission mainly traces high-density clumps. Our result means low gas density for CO-emitting

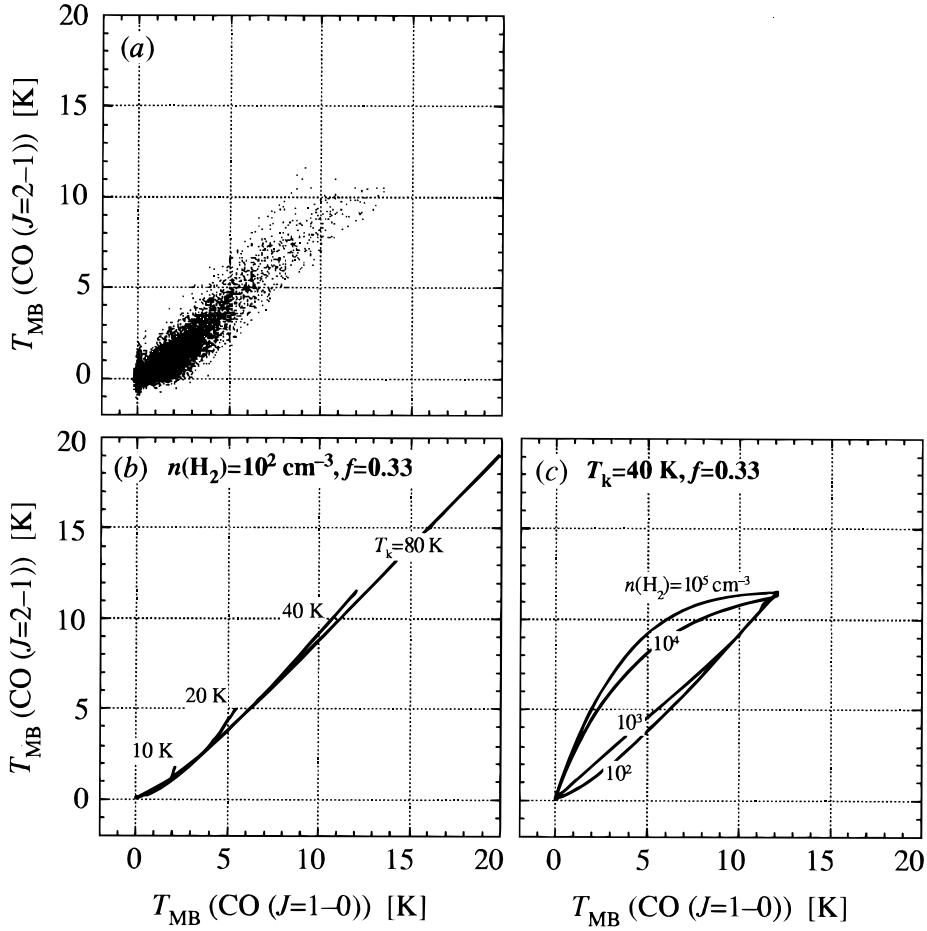

FIG. 11.—(*a*) CO ($J = 1$–0)–CO ($J = 2$–1) intensity correlation plot for the Galactic center molecular cloud complex. Spectrum data binned every 5 km s^{-1} velocity width were used. (*b*) Predicted CO ($J = 1$–0)–CO ($J = 2$–1) intensity correlation based on the one-zone LVG model with $n(H_2) = 10^2$ cm^{-3}, $T_k = 10$, 20, 40, 80 K, and a beam filling factor of $f = 0.33$ for the both lines. (*c*) Same as (*b*), but with $T_k = 40$ K, $n(H_2) = 10^2$, 10^3, 10^4, 10^5 cm^{-3}, and a beam-filling factor of $f = 0.33$ for the both lines.

diffuse clouds even in the Galactic center region despite an abundance of high-density clumps there. The intensity ratio measured here does not follow the general decrease of the ratio with increasing galactocentric distance measured between 4 kpc and 8 kpc mentioned in the previous section. This value is also lower than the median of the $J = 2$–$1/J = 1$–0 intensity ratios toward other galactic nuclei (Braine & Combes 1992).

6.3. *The $J = 2$–$1/J = 1$–0 Intensity Ratios of the Individual Clouds in the Galactic Center*

Figure 12 shows the intensity ratio spectra of the four largest molecular clouds in the Galactic center. These clouds have CO luminosities exceeding 10^6 K km s^{-1} pc^2, which are comparable to those of the largest cloud complexes in the Galactic disk. The total luminosity ratios of these clouds in the Galactic center exhibit very high values compared with those of disk clouds. Shapes of the $J = 2$–$1/J = 1$–0 intensity ratio spectra, not only the total luminosity ratios, considerably differ from those of the disk clouds. However, these discrepancies are mainly due to different definitions for cloud boundary, and hence the above comparison is rather meaningless. The comparison of luminosity ratios or ratio spectra would be meaningful only when they are picked up under the same boundary criterion.

Shapes of $J = 2$–$1/J = 1$–0 intensity ratio spectra of molecular clouds in the Galactic center, as well as the total luminosity ratio, vary from one cloud to another. These differences may be attributed to those in their nature such as physical conditions and environments.

One of them CO $0.0+0.0(+70)$, which contains the $+20$ and $+40$ km s^{-1} cloud, exhibits very high luminosity ratio [$R_{(2-1)/(1-0)} = 1.03$]. This is apparently due to very high abundance of VHRG, which occupies about half of the total luminosity. VHRG in CO $0.0+0.0(+70)$ is distributed in the cloud center as well as in its periphery (Figs. 1, 2). The central concentration of VHRG shows a very large velocity width (Fig. 2) and could be understood as molecular gas close to and exposed to the nuclear region and exposed to its strong UV radiation field.

CO $0.8+0.0(+50)$ and CO $0.9+0.0(+90)$, which contain the active star-forming region Sgr B and the H II region G0.81 $-$ 0.02 (Pauls et al. 1976) respectively, also exhibit high abundance of VHRG. On the other hand, CO $1.4+0.0(+80)$, which contains no H II region, has very small fraction of VHRG. The ratio spectra of these four cloud complexes in the Galactic center clearly demonstrate the close relationship between VHRG and associated UV sources, and support our notion that VHRG is the molecular gas irradiated by strong UV field.

7. CONCLUSION

This paper has presented the results of our off-plane Galactic center survey in the CO ($J = 2$–1) line. We identi-

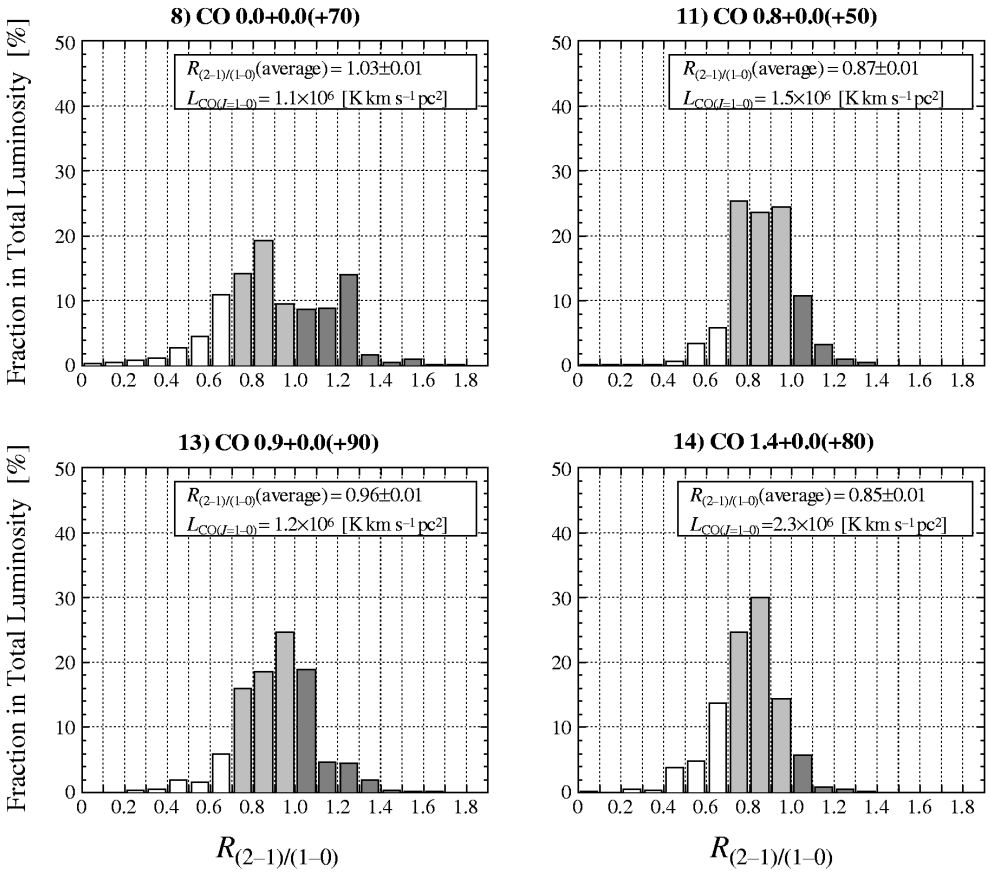

FIG. 12.—The CO ($J = 2$–1)/CO ($J = 1$–0) intensity ratio spectra of the large ($L_{CO}[J = 1$–$0] \geq 10^6$ K km s^{-1} pc^2) molecular clouds in the Galactic center. Spectrum data binned every 5 km s^{-1} velocity width were used. Gases with low ratio (LRG, *white*), high ratio (HRG, *light gray*), and very high ratio (VHRG, *dark gray*) are shown by gray scales.

fied 15 molecular cloud complexes in our data and discussed their dynamical equilibrium using L_{CO}-M_{VT} plots. We also discussed average physical conditions of the molecular gas in the Galactic center in comparison with that in the Galactic disk based on the $J = 2$–$1/J = 1$–0 intensity ratio. The main conclusions are as follows:

1. Molecular cloud layer in the central 400 pc of the Galaxy appears to be gravitationally stable ($Q > 3.4$). This suggests that is it is impossible to form larger molecular cloud complexes, which are observed in the Galactic center, solely by gravitational instability within the gas layer. The other mechanisms, such as collisional buildup of clouds at orbit crowdings, are necessary to promote the growth of the observed large molecular cloud complexes.

The cloud-to-cloud velocity dispersion of ~ 30 km s^{-1} can account for the overall scale height of the Galactic center molecular cloud complex. This suggests that the self-gravity does not play a significant role within the Galactic center molecular cloud complex.

3. The Galactic center molecular cloud complex has subcomplexes of clouds larger than ~ 30 pc. They may not be gravitationally bound but are in equilibrium with the macroscopic external pressure from hot gas and/or magnetic field in this region. Using the expressions of virial mass and CO mass for the pressure bound case, we calibrate the X-factor for the Galactic center molecular clouds as $X = 0.24 \times 10^{20}$ cm^{-2} (K km s^{-1})$^{-1}$. We estimate total molecular mass in the Galactic center as $M(H_2) \cong 2 \times 10^7$ $M_\odot$ as a lower limit; the actual gas mass within the central 400 pc of the Galaxy must be $M(H_2) = (2$–$6) \times 10^7$ $M_\odot$.

4. The total luminosity ratio between $J = 1$–0 and $J = 2$–1 line is $R_{(2-1)/(1-0)} = 0.65 \pm 0.01$ for all emission within $|b| \leq 1°$, $-2.°5 \leq l \leq 2.°5$, and $|V_{LSR}| \leq 150$ km s^{-1}. This indicates that low-density gas dominates the CO luminosity of the central few hundreds parsecs of the Galaxy.

5. Although the CO $J = 2$–$1/J = 1$–0 line intensity ratio is high (~ 0.74) in the midplane, molecular gas at $|b| \geq 0.°25$ exhibits low $J = 2$–$1/J = 1$–0 ratio (~ 0.6). The latitudinal trend is due to the systematic decrease of relative HRG fraction with distance from the Galactic plane.

6. Gas with very high ratios [$R_{(2-1)/(1-0)} \geq 1.0$] exists in the outskirts of cloud complexes in position and velocity. This component may be less dense fluffy clouds in the outskirts of the star-forming ring exposed to intense UV radiation from the ring.

7. The intensity ratio spectra of four large molecular clouds in the Galactic center clearly demonstrate the close relationship between VHRG and associated UV sources. This fact supports our notion that VHRG is the molecular gas irradiated by strong UV field.

We are especially grateful to P. Thaddeus and T. M. Dame for providing the ^{12}CO ($J = 1$–0) data prior to publication. We also thank L. Bronfman and T. Nakano for fruitful discussions. We would like to than the referee, M. L. Kutner, for prompt and helpful comments. The Tokyo-NRO CO ($J = 2$–1) Survey of the Galaxy is a collaborative project between the radio astronomy group of the University of Tokyo and the Nobeyama Radio Observatory (NRO). NRO is a branch of the National Astronomical Observatory, is a radio observing facility open to outside users. We received invaluable supports from many people for the construction of the telescope used for the present survey. N. Kaifu made every effort to realize this collaboration in the earliest stage of this project. K. Sunada was an initial member of this project and played important roles for the establishment of the telescope system. T. O. is financially supported by the Special Postdoctoral Researchers Program of RIKEN. This work was financially supported by the Ministry of Education, Science, and Culture, Japan, under the Grant-in-Aid for Scientific Research on Priority Areas (Interstellar Matter; grant No. 03249205: T. Hasegawa and No. 04233208: T. Hasegawa) and under the Scientific Research Fund (grant No. 01420001: Y. Sofue and 04835004: M. Hayashi), and by Toray Scientific Foundation.

APPENDIX A

LVG MODEL CALCULATIONS

For the transitions with large Einstein A coefficients of the species which is abundant in interstellar space, the radiative process often dominates the excitation of the energy levels (Scoville & Solomon 1974). This process reduces the effective critical density to excite the upper level of transition. The lower J rotational transitions of carbon monoxide are such a case. We have to consider the radiative transfer of lines in the interstellar cloud to calculate the level populations of such a molecule.

The primary purpose of this appendix is to provide the results of the LVG calculation for CO rotational levels in a way many investigators can utilize. A similar attempt has been made by Goldsmith, Young, & Langer (1983).

A.1. *Formulation*

We employed a model with the large velocity gradient approximation (LVG model: Goldreich & Kwan 1974; Scoville & Solomon 1974) to calculate the rotational level populations of carbon monoxide, mainly because of its computational simplicity. This model assumes a large systemic velocity compared with random motions and a uniform velocity gradient along the line of sight. Owing to the highly idealized velocity fields, the level excitations are simplified to a completely local problem.

We solved a set of statistical equilibrium equations (A1) for the first 20 rotational levels of CO. Only the collisions with molecular hydrogen are taken into account. We used the collisional de-excitation rates calculated by Flower & Launcey (1970) for the lower transitions ($J_{upper} \leq 12$). The rates at arbitrary temperatures are calculated from the tables using the spline-interpolation algorithm. For the higher transitions ($J_{upper} > 12$), we used the analytical expression of the collisional

de-excitation rates in de Jong, Chu, & Dargarno (1975). A set of statistical equilibrium equations is

$$f_J \equiv \frac{dn_J}{dt} = \beta_{J+1,J} A_{J+1,J}\left(n_{J+1} - \frac{g_J n_J - g_{J+1} n_{J+1}}{\{\exp\,[2hB(J+1)/kT_{\rm BB}] - 1\}}\right) - \beta_{J,J-1} A_{J,J-1}\left\{n_J - \frac{g_{J-1} n_{J-1} - g_J n_J}{[\exp\,(2hBJ/kT_{\rm BB}) - 1]}\right\}$$
$$+ \sum_{L=J+1}^{N} C_{L,J}\left(n_L - \frac{(2L+1)}{(2J+1)} n_j \exp\left\{\frac{hB}{kT}\,[J(J+1) - L(L+1)]\right\}\right)$$
$$- \sum_{L=0}^{J-1} C_{J,L}\left(n_J - \frac{(2J+1)}{(2L+1)} n_L \exp\left\{\frac{hB}{kT}\,[L(L+1) - J(J+1)]\right\}\right) = 0 \qquad (J = 0, \ldots, N)\,, \tag{A1}$$

where n_J is the fractional number density of molecules in the rotational level J, $T_{\rm BB}$ is the cosmic background radiation temperature, and B is the rotational constant of the molecule. $A_{J+1,J}$ and $B_{J+1,J}$ are Einstein A and B coefficients, and $C_{J,L}$ are collisional de-excitation rates. $\beta_{J+1,J}$ are the escape probabilities from a spherically symmetric cloud (Castor 1970). The escape probabilities are expressed with the optical depths toward cloud center $\tau_{J+1,J}$,

$$\beta_{J+1,J} = [1 - \exp\,(-\tau_{J+1,J})]/\tau_{J+1,J}\,. \tag{A2}$$

Since the equations (A1) does not make a completely independent set, the last equation was replaced with the normalization condition for n_J to get a unique solution,

$$f_N \equiv \sum_{J=0}^{N} n_J = 1\,. \tag{A3}$$

The nonlinear equations (A1) and (A3) were solved iteratively with Newton-Raphson method. In high-density regime, where collisional processes dominate the excitation, less than 20 iterations were necessary for the systems to converge ($|n_J^{(i+1)} - n_J^{(i)}|/n_J^{(i)} < 10^{-10}$ for all J). In the regime of low density and high CO opacity, where radiative processes are dominant, the system converges more slowly because of its strong nonlinear dependence of n_J. In this case typically $\sim$100 iterations are required to reach a solution, or sometimes remains small ($|n_J^{(i+1)} - n_J^{(i)}|/n_J^{(i)} \sim 10^{-8}$) vibration after 1000 iterations.

The excess line intensities in temperature units ($\mathscr{I}_{J+1,J}$), including the line intensities above the cosmic background and optical depths ($\tau_{J+1,J}$) toward the cloud center, are calculated from the solved level populations:

$$\mathscr{I}_{J+1,J} \equiv \frac{\lambda_{J+1,J}^2}{2k}\,(I_{J+1,J} - I_{\rm BB}) = \frac{c^2 (I_{J+1,J} - I_{\rm BB})}{8kB^2 (J+1)^2}\,, \tag{A4}$$

$$\tau_{J+1,J} = \frac{8\pi^3 \mu^2 n({\rm H}_2)}{3h}\,X_{\rm CO}/(dV/dR)(J+1)(n_J - n_{J+1})\,, \tag{A5}$$

where μ is the electric dipole moment of CO, and $I_{J+1,J}$ and $I_{\rm BB}$ are the specific intensities of the line and the cosmic background radiation, respectively. The excitation temperatures $T_{{\rm ex},(J+1,J)}$ are defined by

$$T_{{\rm ex},(J+1,J)} \equiv \frac{2hB(J+1)}{k \ln (n_{J+1}/n_J)}\,. \tag{A6}$$

The excess line intensity $\mathscr{I}_{J+1,J}$ is expressed in these terms as

$$\mathscr{I}_{J+1,J} \equiv \frac{2hB(J+1)}{2k}\,[1 - \exp\,(-\tau_{J+1,J})]\left\{\frac{1}{[\exp\,(2hBJ/T_{{\rm ex},(J+1,J)}) - 1]} - \frac{1}{[\exp\,(2hBJ/T_{\rm BB}) - 1]}\right\}. \tag{A7}$$

A2. RESULTS

We made calculations in the physical parameter ranges of our interest, which are kinetic temperatures (T_k) from 10 to 100 K, molecular hydrogen densities [$n({\rm H}_2)$] from 10 to 10^8 cm^{-3}, and CO fractional abundances per unit velocity gradient [$X_{\rm CO}/(dV/dR)$] from 10^{-10} to 10^{-2} (km s^{-1})$^{-1}$ pc. The parameter steps are 5 K for kinetic temperature and 0.25 dex for the others.

We assumed the isotopic abundance ratio [^{12}CO]/[^{13}CO] = 30 in calculating ^{12}CO (J = 1–0)/^{13}CO (J = 1–0) intensity ratios (hereafter $R_{12/13}$). The standard values of the isotopic abundance ratios are [^{12}CO]/[^{13}CO] = 89 in the solar neighborhood and [^{12}CO]/[^{13}CO] = 28 in the Galactic center (Wannier 1989). Langer & Penzias (1990) reported a lower abundance ratio, [^{12}CO]/[^{13}CO] = 24, toward Sgr B2 cloud. Slight difference in the isotopic abundance does not alter the behavior of $R_{12/13}$ considerably, although the lower [^{12}CO]/[^{13}CO] abundance ratio gives a downward revision to $R_{12/13}$.

We present the results of our calculations in the four illustrations, Figures 13–16. Figure 13 shows contour curves of $R_{(2-1)/(1-0)} \equiv \mathscr{I}_{2-1}/\mathscr{I}_{1-0}$ (*solid lines*) and $\mathscr{I}_{1-0}$ (*broken lines*) as functions of T_k and $n({\rm H}_2)$. Four panels in the figure correspond to $X_{\rm CO}/(dV/dR) = 10^{-4}$, 10^{-5}, 10^{-6}, and 10^{-7} (km s^{-1})$^{-1}$ pc, respectively. Figure 14 also shows contour curves of $R_{(2-1)/(1-0)}$ and $\mathscr{I}_{1-0}$ as functions of $X_{\rm CO}/(dV/dR)$ and $n({\rm H}_2)$. Four panels in the Figure 14 correspond to T_k = 10, 20, 40, and 80 K.

We notice that $R_{(2-1)/(1-0)}$ increases with density in the low-density regime. The level populations approach local thermal equilibrium (LTE) with increasing density. At the limit of high density and optical thickness (upper part of each panel in Fig. 13, upper right part of each panel in Fig. 14), $R_{(2-1)/(1-0)}$ converges to a constant close to unity. Due to the invalidity of

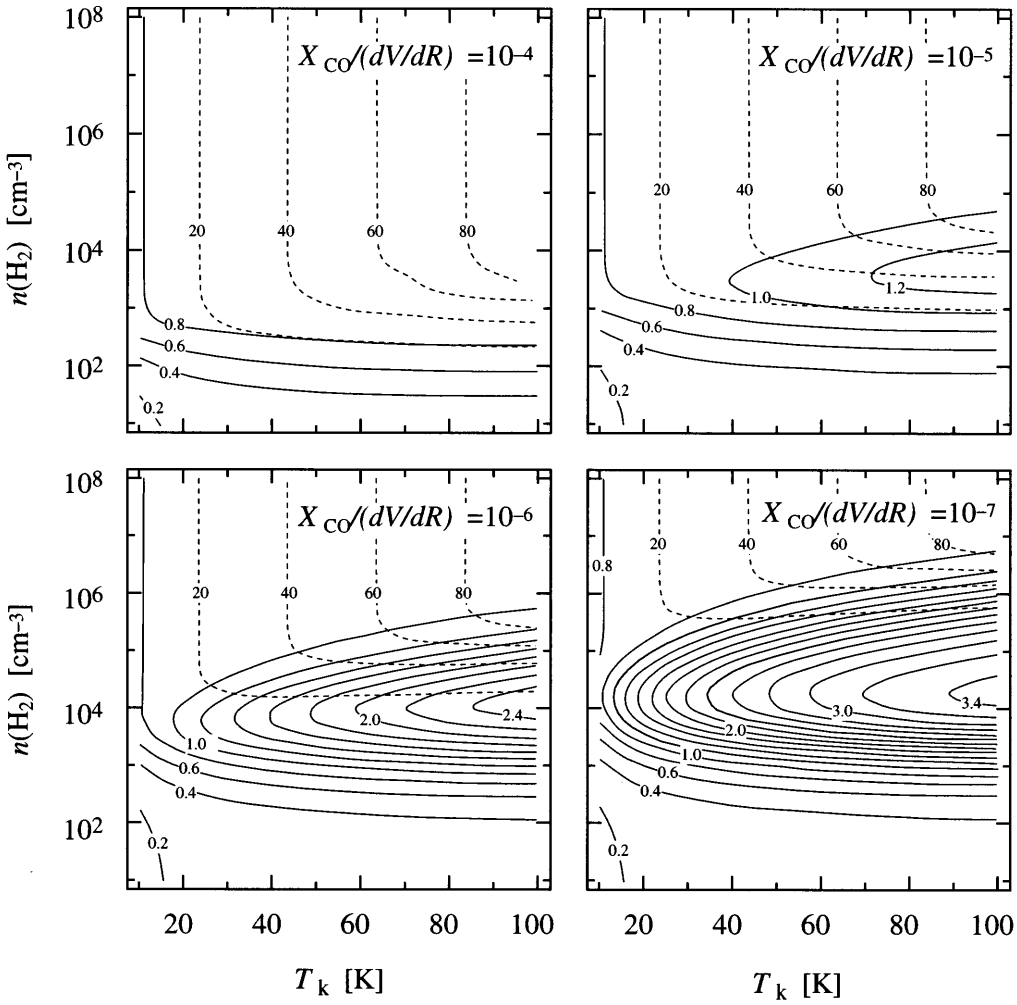

FIG. 13.—Curves of constant $R_{(2-1)/(1-0)}$ (*solid lines*) and $\mathscr{I}_{1-0}$ (*broken lines*) as a function of T_k and $n(H_2)$, for different values of $X_{CO}/dV/dR$. X_{CO} is defined as $[CO]/[H_2]$, and the units of dV/dR are km s^{-1} pc^{-1}.

Rayleigh-Jeans approximation in millimeter-wavelenghts, $R_{(2-1)/(1-0)}$ from optically thick, thermalized gas must always be less than unity. $R_{(2-1)/(1-0)}$ from optically thin, thermalized gas (*upper left part* of each panels in Fig. 14) is greater than unity.

$R_{(2-1)/(1-0)}$ increases monotonously with kinetic temperature, while its dependence to density is more complicated. An increase in kinetic temperature raises the partition function of rotational levels and then reduces each level population. This effect makes each line tend to be optically thin. At the limit of optically thin and high temperature, $R_{(2-1)/(1-0)}$ converges to 4, which is the ratio of optical depths.

In the parameter regime where photon trapping process dominates the excitation (lower right part of each panel in Fig. 14), $R_{(2-1)/(1-0)}$ increases with $X_{CO}/(dV/dR)$ as optical depths of the lines increase. To illustrate the dependence of $R_{(2-1)/(1-0)}$ to optical depths clearly, we plotted $R_{(2-1)/(1-0)}$ as a functon of CO column density per unit velocity width (N_{CO}/dV) and density in Figure 15. Gray curves indicate the line where the optical depth of ^{12}CO ($J = 1$–0) line is equal to unity. We also plotted $R_{12/13} \equiv \mathscr{I}[^{12}CO\ (J = 1\text{–}0)]/\mathscr{I}[^{13}CO\ (J = 1\text{–}0)]$ in Figure 15 assuming the isotopic ratio $[^{12}CO]/[^{13}CO] = 30$. Using this figure, we categorize the state of excitation into the following three characteristic regimes.

1. *Optically thick, thermalized regime.*—Right part of each panel in Figure 115. This regime is the limit of thermalization and optical thickness. At lower density part of this regime, photon trapping process also contributes to level excitation. Typical intensity ratios in this regime are $R_{(2-1)/(1-0)} = 0.8$–0.9 and $R_{12/13} \lesssim 15$ (for $[^{12}CO]/[^{13}CO] = 30$).

2. *Optically thin, thermalized regime.*—Upper left part of each panel in Figure 15. The $J = 2$ level is sufficiently thermalized and each line is optically thin ($\tau \lesssim 3$) in this regime. Typically intensity ratios in this regime are $R_{(2-1)/(1-0)} \gtrsim 1.0$ and $R_{12/13} \gtrsim 15$.

3. *Subthermal regime.*—Lower left part of each panel in Figure 15. The $J = 2$ level is not sufficiently thermalized. The $J = 1$–0 line tends to be optically thick compared to that in the higher density with the same N_{CO}/dV, because most of the molecules reside in the rotational ground state ($J = 0$). Typical intensity ratios in this regime are $R_{(2-1)/(1-0)} \lesssim 0.7$ and $R_{12/13} \gtrsim 15$.

The intensity ratios changes rapidly, often depending on a physical parameter, near the boundaries between the characteristic regimes listed above. $R_{(2-1)/(1-0)}$ increases rapidly with $n(H_2)$ near the boundary between regimes 2 and 3, as the $J = 2$

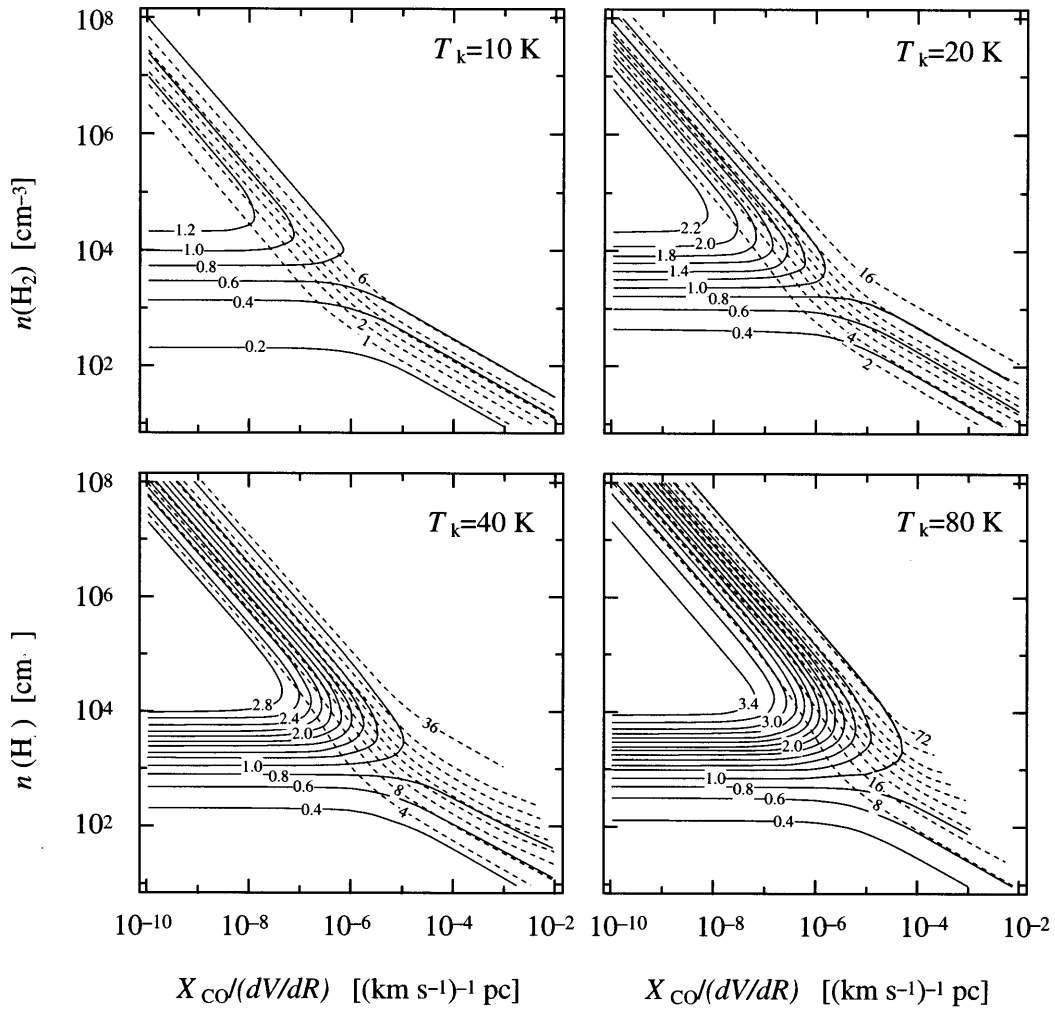

FIG. 14.—Curves of constant $R_{(2-1)/(1-0)}$ (*solid lines*) and $\mathscr{I}_{1-0}$ (*broken lines*) as a function of $X_{CO}/dV/dR$ and $n(H_2)$, for different values of T_k

level is being populated. Near the boundary between regimes 1 and 2, $R_{(2-1)/(1-0)}$ increases rapidly with N_{CO}/dV, with the increasing optical depths. $R_{(2-1)/(1-0)}$ depends on N_{CO}/dV as well as $n(H_2)$ near the boundary between regimes 1 and 3. We can use $R_{(2-1)/(1-0)}$ as a diagnosis for $n(H_2)$ or N_{CO}/dV with an assumed temperature on which $R_{(2-1)/(1-0)}$ monotonically depends.

The behavior of $R_{12/13}$ in N_{CO}/dV–$n(H_2)$ plane is rather simple. $R_{12/13}$ rapidly decreases with increasing N_{CO}/dV, with the increasing optical depths, from regime 2 to 1 and from 3 to 1. $R_{12/13}$ does not change considerably with $n(H_2)$ since there is no significant differences between ^{12}CO and ^{13}CO in the CO-H_2 collisional excitation cross sections. An increase in temperature reduces the optical depths, and thereby increases $R_{12/13}$. $R_{12/13}$ can be a good measure for the optical depths at the density higher than 10^3 cm^{-3}, where the level populations lower than $J = 2$ are nearly in LTE.

A3. *Validity of One-zone Analysis*

We can estimate physical conditions in molecular clouds using the observed line ratios with the help of LVG calculations, under the assumption that emitting regions of each line are roughly identical (one-zone assumption). However, the molecular cloud inevitably contains internal substructures within an instrumental beam of finite size. In addition, there may be a temperature gradient across the surface of molecular clouds that are irradiated by interstellar UV field. Different critical densities and the optical depths of the lines may bring different size of emitting regions accordingly. Here we examine the validity of the one-zone assumption between $J = 1$–0 lines and ^{12}CO and ^{13}CO lines.

The absorption coefficient in the $J = 2$–1 line is generally higher than that of the $J = 1$–0 line if the $J = 2$ level is sufficiently thermalized. In this case, optical depths of each line coincide with those in LTE case and are proportional to CO column density per unit velocity width (N_{CO}/dV). At low density, on the other hand, the $J = 2$–1 line tends to be optically thinner since $J = 1$ level is not sufficiently populated. Figure 16 illustrates the optical depths of the $J = 1$–0 and $J = 2$–1 lines as a function of N_{CO}/dV and $n(H_2)$. We define the "photospheres" of the lines as the closed surfaces where the optical depths measured from the cloud surface become significant ($\tau \sim 3$). Most of the photons escaping from the cloud are emitted around the photosphere. If density does not vary considerably over $\Delta R/\Delta V \sim 0.1$ pc (km s^{-1})$^{-1}$ from the surface, the relative depths and/or sizes of photospheres can be assessed using Figure 16.

The $J = 1$–0 and $J = 2$–1 lines of CO effectively trace the region where the density is about $10^{2.5}$ cm^{-3}, since the energy loss rates per CO molecule peak at $n(H_2) = 10^{2-2.5}$ cm^{-3} over the temperature of our interest ($T_k = 10$–100 K). This density

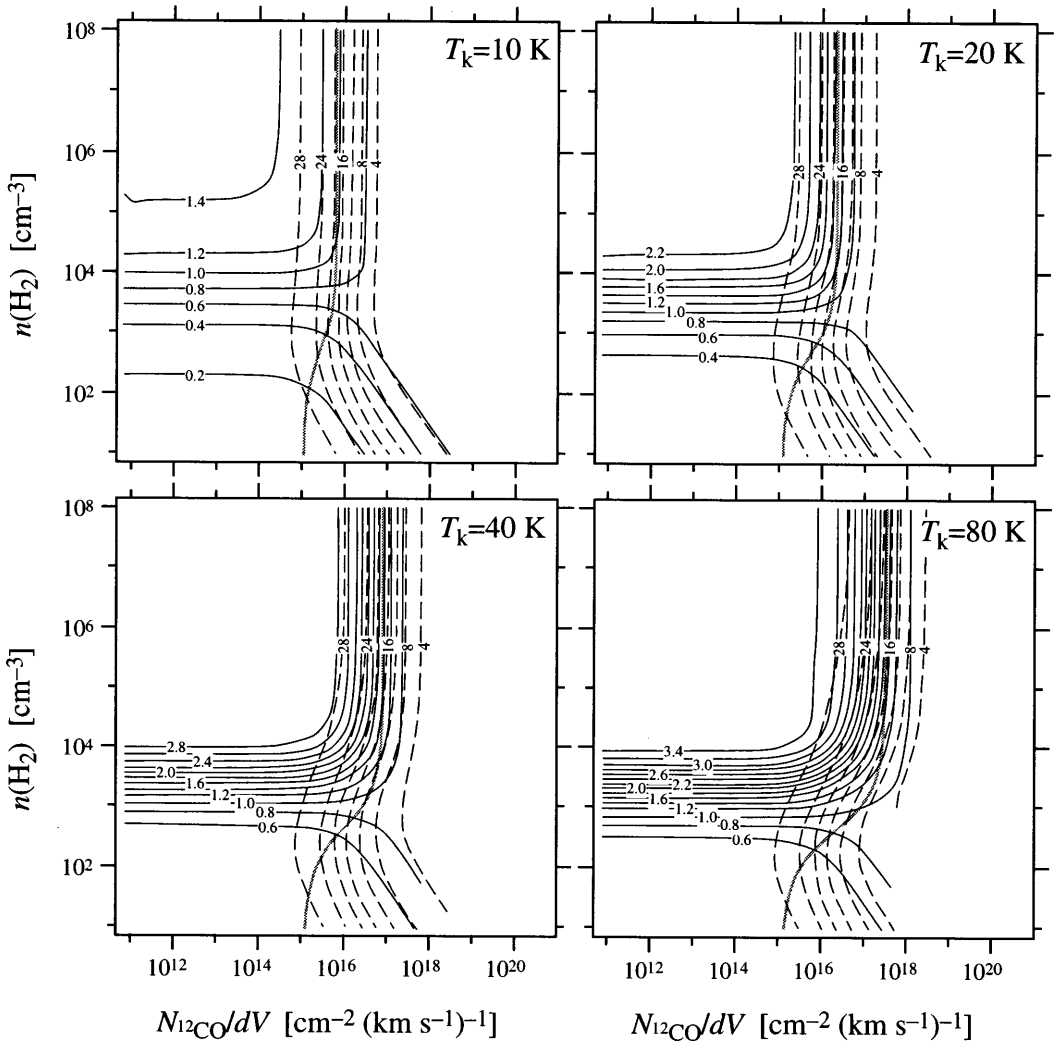

FIG. 15.—Curves of constant $R_{(2-1)/(1-0)}$ (*solid lines*) and $R_{12/13}$ (*broken lines*) as a function of N_{CO}/dV and $n(H_2)$, for different values of T_k. The isotopic abundance [^{12}CO]/[^{13}CO] is set to 30. The units of N_{CO}/dV are km s^{-1} pc^{-1}. Gray curves indicate the line where the optical depth of ^{12}CO (J = 1–0) line is equal to unity.

is typical for the "envelopes" of molecular clouds because they are usually defined in CO (J = 1–0) maps. We confine the following discussion to the density around $n(H_2) = 10^{2.5}$ cm^{-3}.

When gas temperatures is lower than 20 K, the J = 1–0 photosphere resides ouside the J = 2–1 photosphere. At T_k = 10 K, for example, the J = 2–1 photosphere resides $\Delta R/\Delta V \sim 0.06$ pc (km s^{-1})$^{-1}$ from the surface, which is $\sim$1.4 times deeper than the J = 1–0 photosphere. If the CO-emitting gas is in a form of small clumps comparable in size to the depths of the photospheres, different depths to the photospheres lead to a significant difference in beam-filling factors and bring lower $R_{(2-1)/(1-0)}$ than that expected by one-zoner model. The photospheres roughly coincide at T_k = 20 K, which is typical value for giant molecular clouds. In this case, the results of one-zone model correctly reflect the physical conditions in the CO photospheres. At higher temperature, exceeding 20 K, the J = 2–1 photosphere resides outside the the J = 1–0 photosphere and hence results in higher $R_{(2-1)/(1-0)}$ than that expected by one-zone model.

This beam-filling effect makes $R_{(2-1)/(1-0)}$ more sensitive to the kinetic temperature. In addition, there may be a steep temperature gradient across the photospheres of externally heated clumps, and hence the outer photosphere may shine brighter than the inner photosphere. This effect may reduce $R_{(2-1)/(1-0)}$ at lower temperature ($T_k \lesssim 20$ K) and may raise $R_{(2-1)/(1-0)}$ at higher temperatures ($T_k \gtrsim 20$ K). These effects to the intensity ratios have been demonstrated by the numerical model of UV irradiated cloud by Gierens et al. (1992).

However, the above discussion is based on a clumpy molecular cloud model with a temperature gradient across the J = 1–0 and J = 1–0 and J = 2–1 photospheres. If most of the CO emission comes from diffuse cloud which fills over the telescope beam and physical conditions do not vary considerably across the CO photospheres [$\Delta R/\Delta V \sim 0.1$ pc (km s^{-1})$^{-1}$], the one-zone assumption for the J = 1–0 and J = 2–1 lines would be valid to a certain extent.

Between ^{12}CO (J = 1–0) and ^{13}CO (J = 1–0) lines, the one-zone assumption seems to be far from valid for "clumpy" molecular clouds. This is because less opaque ^{13}CO line tends to trace higher column density clumps such as cloud cores while highly opaque ^{12}CO line traces diffuse component such as cloud envelope. The effect of temperature gradient to $R_{12/13}$ would be more serious than that to $R_{(2-1)/(1-0)}$ because of their far different opacities. Only in the case that most of ^{13}CO

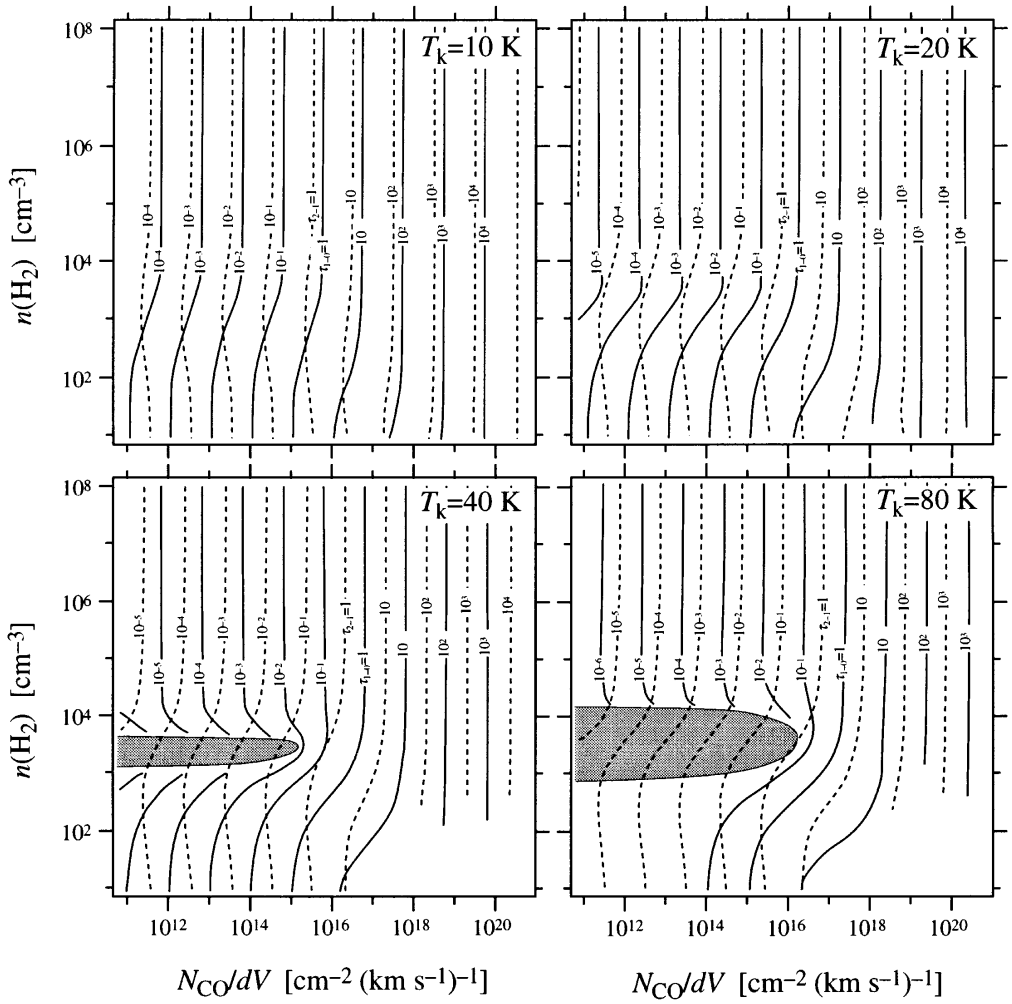

FIG. 16.—Curves of constant optical depths of CO (J = 1–0) line (*solid lines*) and CO (J = 2–1) line (*broken lines*) as a function of N_{CO}/dV and $n(H_2)$, for different values of T_k.

emission also comes from diffuse clouds with low opacity and physical conditions are roughly uniform over the telescope beam, would $R_{12/13}$ approach the values predicted by one-zone calculations.

REFERENCES

Bally, J., Stark, A. A., Wilson, R. W., & Henkel, C. 1987, ApJS, 65, 13
———. 1988, ApJ, 324, 223
Bania, T. M. 1977, ApJ, 216, 381
———. 1986, ApJ, 308, 868
Binney, J., & Tremaine, S. 1987, Galactic Dynamics (Princeton: Princeton Univ. Press)
Bitran, M. E. 1987, Ph.D. thesis, Univ. Florida
Blitz, L., Bloemen, J. B., G. M., Hermsen, W., & Bania, T. M. 1985, A&A, 143, 267
Blitz, L., & Spergel, D. N. 1991, ApJ, 379, 631
Braine, J., & Combes, F. 1992, A&A, 264, 433
Burton, W. B., & Liszt, H. S. 1983, ApJS, 52, 63
Castets, A., Duvert, G., Dutrey, A., Bally, J., & Langer, W. D. 1990, ApJ, 234, 469
Castor, J. I. 1970, MNRAS, 149, 111
Chièze, J. P. 1987, A&A, 171, 225
Clemens, D. P. 1985, ApJ, 295, 422
Cohen, R. S., Dame, T. M., Garay, G., Montani, J., Rubio, M., & Thaddeus, P. 1988, ApJ, 331, L95
Cox, P. & Laureijs, R. 1989, in IAU Symp. 136, The Center of the Galaxy, ed. M. Morris (Dordrecht: Kluwer), 121
Dahmen, G., et al. 1996, in ASP Conf. Ser., the 4th ESO/CTIO Workshop: The Galactic Center, ed. R. Gredel (San Francisco: ASP), in press
de Jong, T., Chu S.-I., & Dargarno, A. 1975, ApJ, 199, 69
Digel, S. W., Hunter, S. D., & Mukherjee, R. 1995, ApJ, 441, 270
Elmegreen, B. G. 1989, ApJ, 338, 178
Flower, D. R., & Launey, J. M. 1985, MNRAS, 214, 271
Fukui, Y., Iguchi, T., Kaifu, N., & Chikada, Y. 1977, PASJ, 29, 643
Genzel, R., Stacy, G. J., Harris, A. I., Townes, C. H., Geis, N., Graf, U. U., Poglitsch, A., & Stutzki, J. 1990, ApJ, 356, 160
Gierens, K. M., Stuzki, J., & Winnewisser, G. 1992, A&A, 259, 271
Goldreich, P., & Kwan, J. 1974, ApJ, 189, 441
Goldsmith, P. F., Young, J. S., & Langer, W. D. 1983, ApJ, 51, 203
Güsten, R. 1989, in IAU Symp. 136, The Center of the Galaxy, ed. M. Morris (Dordrecht: Kluwer), 89
Güsten, R., Walmsley, C. M., & Pauls, T. 1981, A&A, 103, 197
Handa, T., Hasegawa, T., Hayashi, M., Sakamoto, S., Oka, T., & Dame, T. M. 1993, in AIP Conf. Proc. 278, Back to the Galaxy, ed. S. S. Holt, & F. Verter (New York: AIP), 315
Hasegawa, T. 1996, in IAU Symp. 170, CO: Twenty-five Years of Millimeter-wave Spectroscopy, ed. W. B. Latter, S. J. E. Ladford, P. R. Jewel, J. G. Mugnum & J. Bally (Dordrecht: Kluwer), 39
Hayashi, M., Hasegawa, T., Sunada, K., & Kaifu, N. 1990, in Submillimeter Astronomy, ed. G. D. Watt & A. S. Webster (Dordrecht: Kluwer), 63
Hayashi, M., et al. 1997, in preparation
Henkel, C., Baan, W. A., & Mauersberger, R. 1991, A&A Rev., 3, 47
Jackson, J. M., Heyer, M. H., Paglione, T. A. D., & Bolatto, A. D. 1996, ApJ, 456, L91
Kaifu, N., Kato, T., & Iguchi, T. 1972, Nature Phys. Sci., 238, 105

Kent, S. M. 1992, ApJ, 387, 181
Kutner, M. L., & Ulich, B. L. 1981, ApJ, 250, 341
Langer, W. D., & Panzias, A. A. 1990, ApJ, 357, 477
Liszt, H. S., & Burton, W. B. 1978, ApJ, 226, 790
Maloney, P. 1988, ApJ, 334, 761
Mezger, P. G., & Pauls, T. 1979, in IAU Symp. 84, Large-Scale Characteristics of the Galaxy, ed. W. B. Burton (Dordrecht: Reidel), 357
Morino, J. I., et al. 1996, in IAU Symp. 170, CO: Twenty-five Years of Millimeter-Wave Spectroscopy, ed. W. B. Latter, S. J. E. Ladford, P. R. Jewel, J. G. Mugnum & J. Bally (Dordrecht: Kluwer)
Morris, M., Polish, N., Zuckerman, B., & Kaifu, N. 1983, AJ, 88, 1228
Oka, T. Hasegawa, T., Hayashi, M., Handa, T., & Sakamoto, S. 1996a, ApJ, 460, 334 (Paper I)
Oka, T., Hasegawa, T., Sato, F., Tsuboi, M., & Handa, T. 1996b, in IAU Symp. 170, CO: Twenty-five Years of Millimeter-Wave Spectroscopy, ed. W. B. Latter, S. J. E. Ladford, P. R. Jewel, J. G. Mugnum & J. Bally (Dordrecht: Kluwer), 65
Oort, J. H. 1977, ARA&A, 15, 295
Pauls, T., Downes, D., Mezger, P. G., & Churchwell, E. 1976, A&A, 46, 407
Pauls, T., & Mezger, P. G. 1975, A&A, 44, 259
Rubio, M. 1997, in IAU Symp. 170, CO: Twenty-five Years of Millimeter-Wave Spectroscopy, ed. W. B., Latter, S. J. E. Ladford, P. R., Jewel, J. G. Mugnum, & J. Bally (Dordrecht: Reidel), 265
Rubio, M., Garay, G., Montani, J., & Thaddeus, P. 1991, ApJ, 368, 173
Rubio, M., Lequeux, J., & Boulanger, F. 1993, A&A, 271, 9
Sakamoto, S., Hasegawa, T., Hayashi, M., Handa, T., & Oka, T., 1994, ApJ, 475, 641
———. 1995, ApJS, 100, 125
Scoville, N. Z. 1972, ApJ, 175, L127
Scoville, N. Z., & Solomon, P. M. 1974, ApJ, 187, L67
Sharpless, S. 1959, ApJS, 4, 257
Solomon, P. M., Rivolo, A. R., Barret, J., & Yahil, A. 1987, ApJ, 319, 730
Sorai, K., et al. 1996, in Proc. East Asian Meeting on Astronomy, ed. N. Kaifu, (Tokyo: National Astronomical Observatory), 115
Spergel, N., & Blitz, L. 1992, Nature, 357, 665
Tsuboi, M., et al. 1997, ApJS, submitted
Vogel, S. N., Boulanger, F., & Ball, R. 1987, ApJ, 321, L145
Wannier, P. G. 1989, in IAU Symp. 136, The Center of the Galaxy, ed. M. Morris (Dordrecht: Kluwer), 107
Wilson, C. D., & Reid, I. N. 1991, ApJ, 366, L11
Wilson, C. D., & Scoville, N. 1990, ApJ, 363, 435
Yamauchi, S., Kawada, M., Koyama, K., Kunieda, H., & Tawara, Y. 1990, ApJ, 365, 532
Young, J. S., & Scoville, N. Z. 1991, ARA&A, 29, 581
Zylka, R., Güsten, R., Henkel, C., & Batrla, W. 1992, A&AS, 96, 525